



eBook

# mmWave Design Guide

October 2019

SPONSORED BY



### 3 Introduction

---

Pat Hindle  
*Microwave Journal, Editor*

### 4 mmWave Will Be The Critical 5G Link

---

Joe Madden  
*Mobile Experts, Campbell, Calif.*

### 8 From Waveforms to MIMO: 5 Things for 5G New Radio

---

Alejandro Buritica  
*National Instruments, Austin, Tex.*

### 11 Using GDF to Assess 5G Antenna Directionality

---

Scott Langdon  
*Remcom Inc., State College, Pa.*

### 14 Characterizing Circuit Materials at mmWave Frequencies: Part I

---

John Coonrod  
*Rogers Corp., Chandler, Ariz.*

### 19 Characterizing Circuit Materials at mmWave Frequencies: Part II

---

John Coonrod  
*Rogers Corp., Chandler, Ariz.*

## mmWave Design Guide

For many years mmWave technology has been reserved for specialized applications and expensive to manufacture. But with the proliferation of automotive radar, 5G FR2 applications, and higher frequency satellite communication systems, mmWave technology has becoming mainstream and the cost to manufacture systems is coming down rapidly as new architectures are developed, and volumes increase.

Designing the antenna system is a critical part of any mmWave product as the size of the elements is small enough to be integrated into the packaging and typically very close to the circuits to minimize losses. This eBook takes a look at the importance of mmWave technology and the design considerations needed for antenna and system design. The first two articles discuss mmWave technology related to 5G NR systems. Then we look at antenna simulation for better design of systems using CDF to assess 5G antenna directionality. The last two articles cover the PCB material considerations for designing circuits at mmWave frequencies and takes a comprehensive look at the subtle effects that need to be understood to properly design systems.

Thanks to Rogers Corporation for sponsoring this eBook to bring it to readers for free. We hope that these insights will help in the design of your future systems.

*Pat Hindle, Microwave Journal Editor*



# mmWave Will Be The Critical 5G Link

Joe Madden  
 Mobile Experts, Campbell, Calif.

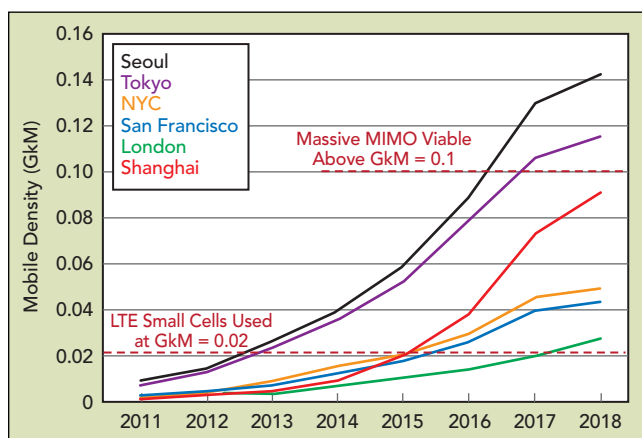
Over the past 30 years, the mobile network has become a critical part of life, and the use of mobile services is starting to reach incredible levels of demand. This year, 30 Exabytes will fly over worldwide mobile networks every month. And the demand will continue to rocket upward by roughly 50 percent each year. About 15 percent of adults in the U.S. use LTE full-time, leaving Wi-Fi turned off (they say that managing Wi-Fi hotspots can be annoying). A whole generation of young people consumes 50 GB of mobile video each month, relying on “unlimited plans.” The signs are clear that data demand will continue to grow rapidly.

Mobile Experts tracks the demand for mobile data with multiple mobile operators worldwide and their Traffic Density tracking metric measures the level of traffic in a busy sector, during busy hours, in terms of Gigabits per second, per square kilometer, per MHz of spectrum (GkM). In order to understand how advanced networks should handle extreme demand in some cities, the GkM is compared between different operators, and an assessment can be made whether small cells, massive MIMO or mmWaves will be necessary to accommodate the traffic (see **Figure 1**).

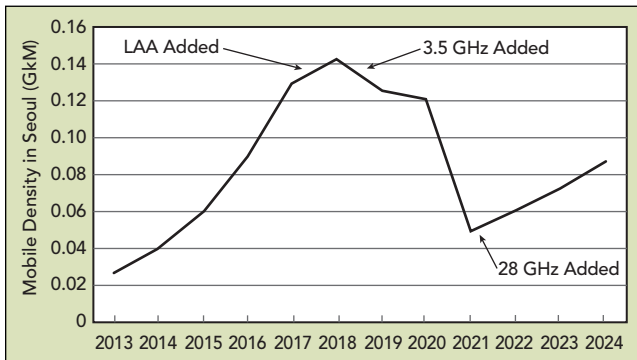
Traffic density in GkM has been rising steadily for years, and is most pronounced in locations such as subway stations in Tokyo and Seoul, where thousands of people stand close together, all watching video. The statistical rise in density has been remarkably smooth as new apps and video content become available on mobile platforms.

Above a traffic density level of 0.02 GkM, small cells were observed to be universally adopted by mobile operators. In other words, the macro network saturated above 0.02 GkM, and small cells became a more economical way to add capacity. More recently, networks have reached levels of density above 0.1 GkM, making massive MIMO necessary to continue increasing capacity.

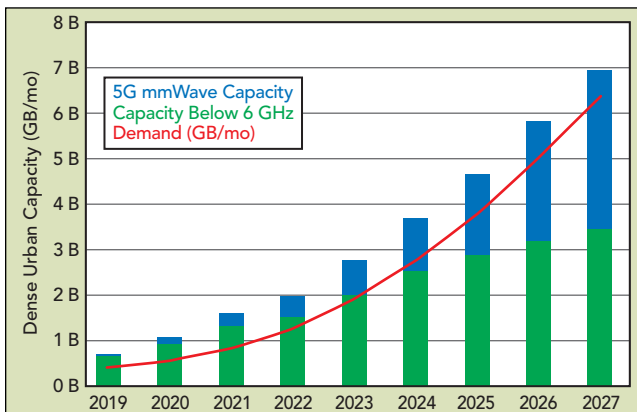
We are now starting to see some signs that density levels in the range of 0.15 to 0.2 GkM will saturate the OFDM network. There will be ways to push through this barrier as well, but moving beyond 0.2 GkM in the 1



▲ Fig. 1 Benchmarking data for Mobile Traffic Density (Gbps/km<sup>2</sup>/MHz or GkM).



▲ Fig. 2 Changes in traffic density with addition of 5G spectrum.



▲ Fig. 3 Demand vs. capacity for dense urban mobile networks in U.S.

to 3 GHz bands will get very expensive, requiring large numbers of very low-power radio nodes.

Adding 5G spectrum to the mobile network can actually reduce the traffic density. As an example, one of the leading Korean networks should experience a drop in GkM with their recent introduction of 100 MHz at 3.5 GHz. An additional 800 MHz of spectrum at 28 GHz will reduce their traffic density in key hotspots to much more manageable levels as shown in **Figure 2**.

Therefore in many ways the operators can be viewed as using 5G spectrum to manage the density of their traffic. When high density makes adding capacity expensive, adding more spectrum is the best option.

### mmWAVES TO THE RESCUE

After the convenient licensed bands below 5 GHz are used up, mobile operators start to look to mmWave spectrum as an opportunity to get significant bandwidth. The U.S. is a prime example where wide blocks of C-Band spectrum are not available so mobile operators have invested heavily in 28 and 39 GHz mmWave bands.

In fact, the large U.S. mobile networks, in key urban pockets, are running out of capacity below 6 GHz. During special events such as the Super Bowl, the traffic density is in the range of 0.12 GkM and above in the U.S. Mobile Experts modeled the demand for mobile data in four segments of the U.S. network (dense urban, urban, suburban and rural) and estimated the total capacity of the mobile network including macro base stations, small cells, CBRS, LAA and the impact of massive

MIMO below 6 GHz. Even with a fully utilized heterogeneous network with maximal capacity, demand in dense urban pockets will exceed capacity in 2023 as shown in **Figure 3**. Note that the numbers shown in the Figure 3 represent the total demand and capacity for all dense urban sites in the U.S., so the extreme high-density locations such as Times Square will experience demand higher than capacity in the 2021 to 2022 timeframe. Extrapolating the trends in traffic density benchmarks, the dense urban sites in New York City should reach daily peak-hour density levels in the range of 0.1 GkM or higher by 2022.

### HOW mmWAVE LINKS CAN BE USEFUL

Many experienced RF engineers have reasonable doubts about using mmWave radio links in a mobile environment. After all, the mmWave link depends on a narrow beam in order to achieve a reasonable link budget. Any clutter in the RF channel can disrupt the narrow beam.

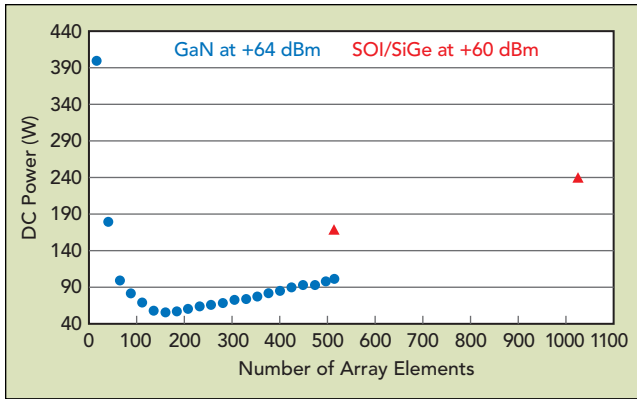
Handovers in a mobile 5G mmWave network have been demonstrated in test systems in Seoul and at speeds above 200 km/hr on a racetrack, so the 5G frame structure lends itself to handovers in extreme Doppler shift conditions.

However, the mobile operators will not be using the 5G mmWave link as a standalone (SA) radio channel initially. Instead, an LTE carrier at 1 to 2 GHz will be used as the primary link, with control signaling taking place on the more reliable lower band. Then, the mmWave link will come into play when it is available to download or upload large amounts of data. In this way, the mmWave radio will add throughput as a carrier aggregation layer, boosting speed when it is available but not essential to the continuity of the link for handovers. At some point, operators may decide to use 5G mmWave as a SA mobile network, but today none of the active operators are planning to operate 5G mmWave independently.

### RF IMPLEMENTATION—INFRASTRUCTURE

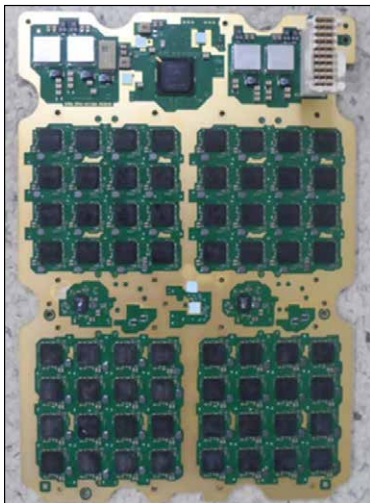
The mmWave base station will look dramatically different than LTE base stations below 6 GHz. At a fundamental level, the mmWave radio suffers from the lower power amplifier efficiency in the 24 to 40 GHz bands, so the level of conducted output power will be much lower than lower frequency mobile radios. The primary limitation is the level of heat dissipation possible in a passively cooled radio unit at the towpotop. Given a limit of about 250 W of heat in a small enclosure, the conducted RF power will be very low, below 10 W in any configuration.

As a result, systems engineers have turned to massive MIMO architectures with at least 64 antennas, in order to use high antenna gain. Initial products have utilized between 64 and 256 antenna elements per beam, to achieve between 25 and 30 dBi of antenna gain. In this way, the low conducted power can achieve linear EIRP in the range of 60 dBm. Each beam also carries multiple streams. Massive MIMO base stations are configured with dual-polarized antenna arrays, so that each beam can operate with 2x2 MIMO.



▲ Fig. 4 Comparison of power dissipation in GaN, SOI and SiGe arrays.

Multiple beams can be supported from a radio unit by constructing the array with multiple panels. From a manufacturing point of view, OEMs are settling into the use of panels with a set number of elements (examples range from 64 to 256 elements per panel). Then, the product can be scaled up and down to support different levels of capacity. One example in the field now uses four 256-element panels for a total of 1024 antenna elements, supporting four beams and 2x2 MIMO in each beam.

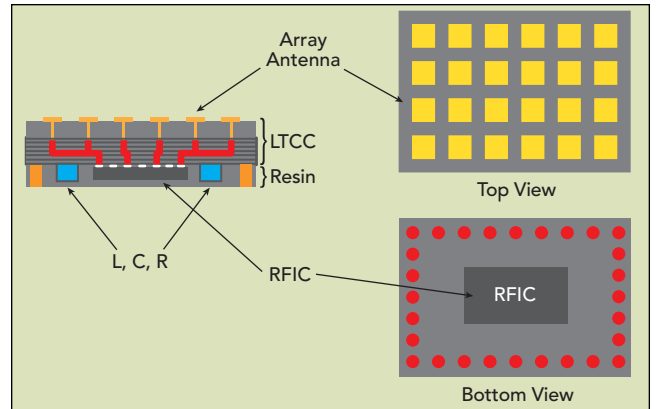


▲ Fig. 6 A typical panel with 4 sections, 64 256 dual-polarized antennas total (Source: FCC filing).

Note that the configuration of beams and streams is not set based on hardware. The OEM can choose to change the configuration in software, assuming that the antenna elements are equipped with analog phase shifter and variable gain components that can be individually controlled. In almost all prototypes, this “hybrid beamforming” approach is used today, as full digital beamforming at very wide bandwidths can be costly in terms of processing power and dollar cost.

Currently, SOI and SiGe semiconductor technologies are used in many base stations in order to achieve high levels of integration and low-cost. GaN also holds great potential for lower power dissipation at high levels of EIRP, using the higher inherent linearity/power of GaN devices to achieve 60 dBm or higher with fewer antenna elements.

Based on PA efficiency data and size/efficiency of heatsinks for live demonstrations at MWC Barcelona 2019, the DC power consumption of multiple mmWave arrays was estimated as shown in **Figure 4**. It appears that GaN has a significant advantage in terms of raw efficiency of a linear power amplifier at 28 GHz. However, all major OEMs have chosen to use SOI or SiGe so far,



▲ Fig. 5 A diagram representing physical packaging/integration for mmWave front ends (source: pSemi).

to take advantage of higher levels of integration, larger wafers and the resulting lower cost profile.

Over the next five years, significant adjustments are expected to occur to the balance between narrow beams (for long range) and wide beams (for better mobility). The optimal tradeoff in a dense urban network is not well understood today, and is likely to break into specific configurations to handle trains/buses/moving vehicles differently than pedestrian users. In particular, the large SOI-based arrays are expected to support the applications that cover dense urban pockets, where both vertical and horizontal steering are required and pedestrian speeds are typical. Other applications with higher mobility and less vertical steering are likely to move toward GaN devices.

The physical integration of the RF front-end will also be critical. Very tight integration will be necessary in the 24 to 40 GHz bands to keep insertion losses low, so either LTCC or 3D glass structures will be used to embed the active die and passive elements (see **Figure 5**).

In the Radio Unit (RU), one convenient arrangement is to use an RFIC device for four antenna elements. From a simple geometric point of view, one RFIC for beam-forming (phase and amplitude adjust) can be positioned between four antenna elements, using short traces and vias to route the mmWave signal (see **Figure 6**).

One open question concerns the use of filters in the mmWave front-end. Currently, no bandpass filters are used at the front-end, and during field trials the spectrum was clean enough to rely on the natural rolloff of the patch antenna and distributed antenna feed to provide out-of-band rejection. In the future, spectrum auctions and multi-operator deployment suggest that interference will arise. In fact, with high EIRP and very narrow beams, the interference will be intense when it unexpectedly pops up. Recent analysis indicates that filters will be introduced into the packaging over the next three years.

## RF IMPLEMENTATION—CPEs

In fixed wireless, the Customer Premises Equipment (CPE) is a key part of the system. Initial deployments of 5G mmWave networks rely on high antenna gain and high EIRP from the CPE in order to support the necessary capacity. CPE RF front-ends today are constructed

using a method that is similar to the network infrastructure, with a panel of antenna elements supported by beamforming RFICs, up-/down-conversion and then baseband processing. A typical CPE uses 32 dual-polarized antenna elements, supporting 2x2 MIMO with about 20 dBi gain from the antenna system.

Because the CPE is always connected to prime power, the PA efficiency is not a crippling limitation, and the CPE can often achieve high gain and high transmit power (linear EIRP in the range of 40 dBm).

## RF IMPLEMENTATION—HANDSETS AND OTHER MOBILE DEVICES

The biggest challenge facing the 5G mmWave link will come from the user's hand blocking the antennas on a smartphone. In the 28 GHz band, the user's hand is likely to attenuate the signal by at least 30 to 40 dB, effectively killing the link altogether. There can be multiple strategies to avoid this issue:

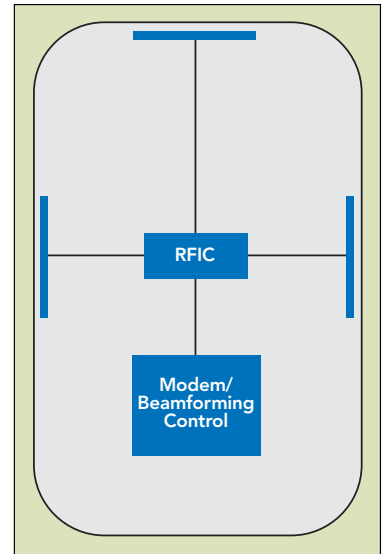
1. Multiple antenna sub-arrays on each handset. All 5G mmWave handset prototypes demonstrated over the past year utilize multiple sub-arrays, placed on both sides of the smartphone.
2. Foldable handsets are coming to market such as Samsung's Galaxy Fold and Huawei's Mate X. Because a foldable handset would be much larger than a human hand in the unfolded position, the placement of antennas could be more exposed.
3. Mobile hotspots can be used instead of mmWave links directly to the smartphone. This avoids the hand issue altogether, but may incur greater interference in the unlicensed bands. Importantly, the space and battery size constraints of the smartphone do not apply here, so the number of antennas can be increased to achieve much higher EIRP.

The physical implementation on a handset is limited for cost and space reasons to a few sub-arrays, an RFIC and the modem/beamforming processing. To make this arrangement economical, each mmWave sub-array includes an up-/down-converter to shift the mmWave signal down to an IF frequency at roughly 4 to 6 GHz (see **Figure 7**). This enables the signals to travel through the PCB to a centralized RF transceiver.

Each mmWave subarray currently uses four dual-polarized patch antennas, each with a transmit/receive switch, low noise amplifier (LNA) and power amplifier (PA) closely integrated using RF-SOI. Each amplifier can only produce about 15 dBm linear power, so as many as eight antennas would be used to reach EIRP levels somewhere above 20 dBm. Three-dimensional beamforming on the smartphone platform is challenging, especially with a cluttered environment with metal surfaces and human hands in very close proximity. Even with eight antennas engaged, prototyping so far suggests antenna gain of only about 5 dBi.

For that reason, we expect much higher performance with hotspot products that utilize 32 antennas or more, achieving gain in the range of 20 dBi in the antenna system (15 dBi from the array and 5 dBi from the patch antenna itself). This type of product should be

able to reach roughly 35 dBm linear EIRP or higher. From a system point of view, roughly 35 dBm or higher will be an important level to reach since the 5G link requires a closed loop with TDD channel feedback in order to maintain a continuous connection. Lower EIRP from the client device means a shorter range for the link, and would require the network operator to deploy larger numbers of cell sites in order to blanket a neighborhood with coverage. In short, low transmit power from the client devices would make the 5G business case unworkable for the mobile operator.



▲ **Fig. 7** Layout of three mmWave sub-arrays on a handset.

## COMMERCIAL STATUS

Base station deployment is underway in earnest for the U.S. market this year, and the South Korean market is not far behind. Recent forecasts indicate that more than 600,000 radio heads will be deployed by 2024.

Commercial fixed-wireless services have already been launched in a handful of U.S. cities, with CPEs supported by major OEMs today. A few CPEs have appeared from the ODM community with poor performance, but we expect those to improve quickly to support healthy growth. In the next few years, the fixed-wireless application will account for millions of users.

This generation of technology is also unique in that handsets are coming out very quickly, and smartphones will be available before the network is launched in most countries. The first 5G mmWave handset has already been released (the 5G Moto MOD), and at least eight other mmWave handsets will be released in the second half of 2019.

## SUMMARY

5G mmWave radio links are more complex, more expensive and less reliable than LTE connections at 1 to 2 GHz. But mmWave bands will be necessary to keep up with rising demand, so the industry is currently pouring money into deployment of base stations and development of client devices. Initial fixed-wireless performance with CPEs has been surprisingly solid. The migration to mobile 5G usage will be tricky, with tradeoffs on beamwidth, link budget, mobility and cost coming into play. But there is one clear conclusion: 5G mmWave will be a significant part of future mobile networks. ■

# From Waveforms to MIMO: 5 Things for 5G New Radio

Alejandro Buritica  
National Instruments, Austin, Texas

**5** G New Radio (NR) is comparable to the mobile communications industry using LTE to describe 4G technology or Universal Mobile Telecommunications Service (UMTS) to describe 3G. As a start, the release 15 specifications for 5G NR were approved in June 2018. These will continue to evolve to cover the detailed technical functionality of Standalone (SA) access for 5G NR devices.

Here are five key technical aspects of the 5G physical layer that enable this global communications standard to deliver an abundance of reliable, data rich and highly connected applications.

## 5G NR WAVEFORMS

1

### CP-OFDM: Downlink and Uplink

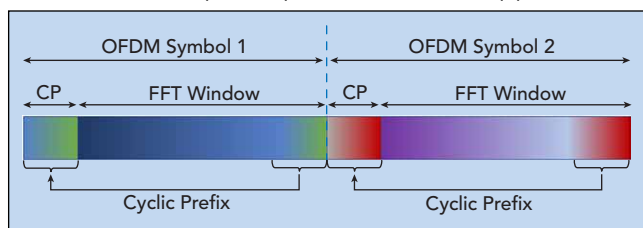
Researchers have been investigating different multicarrier waveforms in recent years, proposing many for 5G radio access. Waveforms that use orthogonal frequency division multiplexing (OFDM) work well for time division duplex operation. They support delay-

sensitive applications and have demonstrated successful commercial implementation with efficient processing of ever-larger bandwidth signals. Also, the high spectral efficiency and MIMO compatibility of OFDM signals help meet the extreme data rate and density coverage needs of this new global cellular communications standard.

Thanks to channel estimation and equalization techniques, OFDM waveforms demonstrate great resiliency in frequency-selective channels. By attaching a copy of the end of the OFDM symbol to the beginning of the symbol (a cyclic prefix), a receiver can better tolerate synchronization errors and prevent intersymbol interference (see **Figure 1**). So the 3GPP settled on using the cyclic prefix OFDM (CP-OFDM) as the waveform for 5G downlink and uplink for modulation schemes up to 256-QAM.

### DFT-S-OFDM: Higher Efficiency Uplink

OFDM waveforms suffer from high peak-to-average power ratios (PAPR). Because the RF power amplifier consumes the most power in a mobile device, system designers wanted a waveform supporting high efficiency amplifier operation while meeting the spectral demands of 5G. For uplink (i.e., user to base station), NR offers user equipment (UE) the option of using CP-OFDM or a hybrid format waveform called discrete Fourier transform spread OFDM (DFT-S-OFDM). Using DFT-S-OFDM, the transmitter modulates all subcarriers with the same data (see **Figure 2**). It lowers the peak-to-average ratio while retaining the multipath interference resiliency and flexible subcarrier frequency allocation



▲ Fig. 1 A CP-OFDM symbol contains a cyclic prefix on each side of the data.



OFDM provides. Where the PAPR with CP-OFDM may be 11 to 13 dB, with DFT-S-OFDM it is only 6 to 9 dB.

## 2

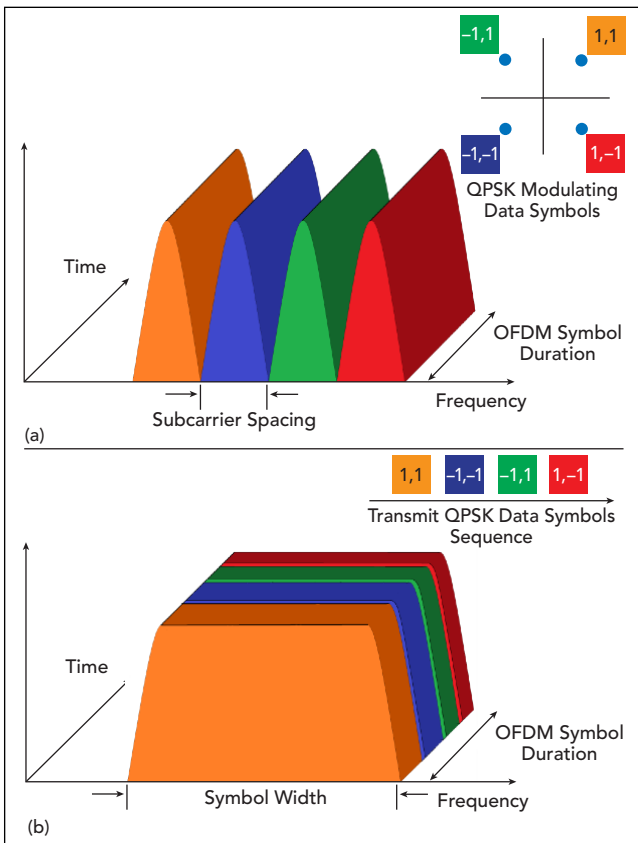
### FLEXIBLE SUBCARRIER SPACING, FRAME STRUCTURE

Operation in multiple frequency bands is a new aspect of 5G NR, from the existing cellular bands below 3 GHz, to wider bands between 3 and 5 GHz, to the mmWave spectrum. **Figure 3** shows the current bands defined for NR operation above 6 GHz.

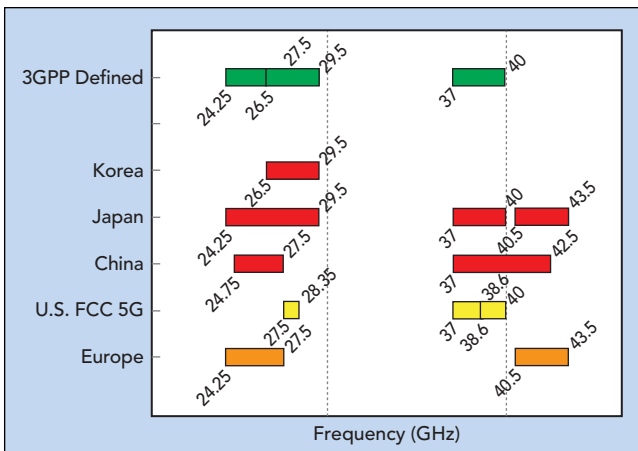
As the carrier frequency increases, so does system phase noise. For example, the difference in phase noise

between carriers at 1 and 28 GHz is about 20 dB. This increase makes it difficult for a mmWave receiver to demodulate an OFDM waveform with the narrow, fixed subcarrier spacing (SCS) and symbol duration of LTE. Also, with moving users, the channel coherence time decreases as the carrier frequency increases because of the Doppler shift, meaning the system has less time to measure the channel and finish a single slot transmission at higher carrier frequencies. Using a narrow subcarrier spacing at mmWave results in unacceptably high error vector magnitude, with considerable performance degradation.

To address these challenges, the 3GPP standardized on a flexible subcarrier spacing that scales the space between orthogonal subcarriers, starting with the 15 kHz subcarrier spacing used for LTE and going to 30, 60 or 120 kHz spacing at mmWave. Leveraging the LTE numerology ensures NR deployments will coexist and be time-aligned with LTE networks.



▲ Fig. 2 Time and frequency comparison of OFDM (a) and DFT-S-OFDM (b).



▲ Fig. 3 NR bands above 6 GHz.

## 3

### MIMO

To increase capacity and spectrum efficiency, 5G NR uses the distributed and uncorrelated spatial locations of multiple users. Using multiuser MIMO (MU-MIMO) technology, the base station (gNB) simultaneously sends data streams to different users, maximizing the signal strength at each user's location while reducing the signal strength (creating nulls) in the directions of the other receivers. This enables the gNB to talk with multiple UEs independently and simultaneously (see **Figure 4**).

### mMIMO for 5G

Massive MIMO (mMIMO) refers to a communications scenario with many more gNB antennas than users. A large difference between gNB antennas and UEs can yield huge gains in spectral efficiency, enabling the communications system to simultaneously serve many more devices within the same frequency band than today's 4G systems (see **Figure 5**). Industry leaders have demonstrated the viability of mMIMO systems for 5G using software defined radio and flexible software, which enable rapid wireless system prototyping.<sup>1</sup>

## 4

### mmWAVE FOR 5G

5G systems operating at 28 GHz or other mmWave bands have the advantage of more available spectrum, enabling larger channels. While the mmWave bands have less spectral crowding than the bands below 6 GHz, communications systems using at these frequencies must contend with very different propagation effects: higher free-space path loss and atmospheric attenuation, weak indoor penetration and poor diffraction around objects. To overcome these undesired effects, mmWave antenna arrays focus their beams and take advantage of antenna array gain. Fortunately, the size of these arrays decreases as the frequency increases, enabling a mmWave antenna array with many elements to be roughly the same size as a single, sub-6 GHz element (see **Figure 6**).

As noted, the channel coherence time decreases significantly at mmWave frequencies, placing tough restrictions on UE mobility applications. As researchers continue to investigate new ways to improve mobility at mmWave, the first 5G mmWave deployments will likely serve fixed wireless access applications such as home broadband, backhaul and sidelink.

- in *Communications*, Vol. 35, No. 8, August 2017, [ieeexplore.ieee.org/abstract/document/7938334/](https://ieeexplore.ieee.org/abstract/document/7938334/).
- 3GPP Technical Specification Group Radio Access Network, "NR, Physical Layer Procedures for Control," TS 38.213 V15.0.0, <https://portal.3gpp.org/desktopmodules/Specifications/SpecificationDetails.aspx?specificationId=3215>.

## 5

### BANDWIDTH PARTS

As 5G applications grow, the diversity of devices and equipment will have to operate successfully across many different bands with varying spectrum availability. One example is the situation where a UE with limited RF bandwidth operates beside a more powerful device that can fill a whole channel using carrier aggregation and a third device that can cover the whole channel with a single RF chain.<sup>2</sup>

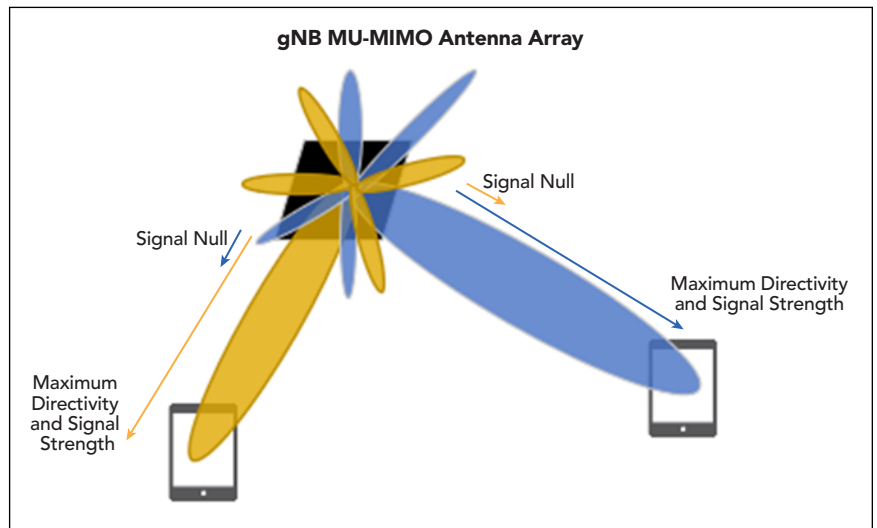
While wide bandwidth enables higher data rates for users, it comes with a cost. If UEs do not need high data rates, using wider bandwidth than required is an inefficient use of the RF and baseband processing resources. 5G NR introduces the concept of bandwidth parts (BWP), where the network negotiates for a certain UE to occupy one wideband carrier, separately configuring other UEs with a subset of contiguous resource blocks. This allows a greater diversity of devices with varying capabilities to share the same wideband carrier. This flexible network operation adjusting to the differing RF capabilities of UEs does not exist with LTE.

### SUMMARY

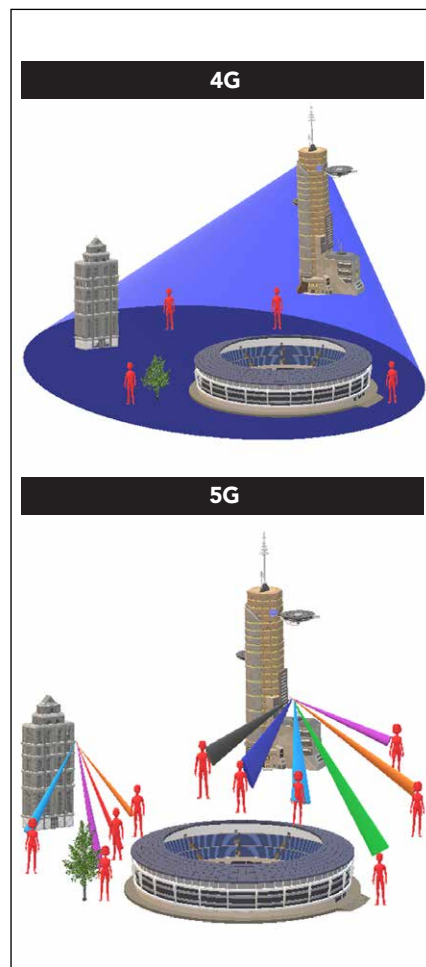
Thanks to higher bandwidth channels and multiple numerology options, NR systems will operate in both sub-6 GHz and mmWave bands, appropriately handling multipath delay spread, channel coherence time and phase noise. NR leverages the latest developments in mMIMO and beamforming to maximize spectral efficiency and provide better quality of service for a larger number of users. Although creating the next generation of 5G devices presents significant design and test challenges, a platform-based approach to design, prototype and test these new wireless technologies is key to 5G becoming a reality within the next decade. ■

### References

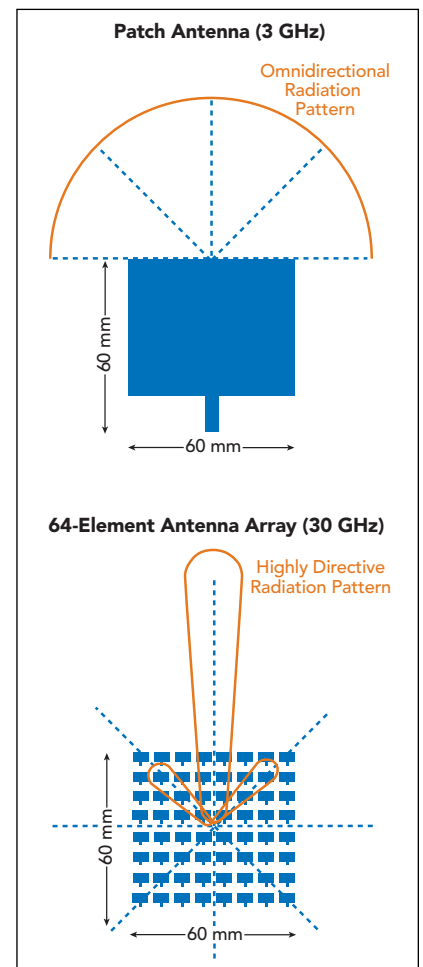
- G. Xu, T. Li et al., "Full Dimension MIMO (FD-MIMO): Demonstrating Commercial Feasibility," *IEEE Journal on Selected Areas*



▲ Fig. 4 Spatial multiplexing using MU-MIMO.



▲ Fig. 5 Spatial multiplexing with mMIMO increases gNB capacity.



▲ Fig. 6 64-element array at 30 GHz has the same size aperture as a single 3 GHz patch antenna.

# Using CDF to Assess 5G Antenna Directionality

Scott Langdon  
Remcom Inc., State College, Pa.

Three of the goals for 5G mobile communications networks are to increase data capacity, decrease latency and connect many more devices. mmWave frequencies with large channel bandwidths are being used to help meet these needs. Indeed, release 15 of the 3GPP 5G specification includes frequencies in the 28 and 38 GHz bands. Drawbacks of these higher frequencies are increased path loss in clear air, in air with precipitation and in environments with higher reflectivity—especially with larger cells outside of dense urban environments.<sup>1</sup>

Fortunately, the shorter mmWave wavelengths enable more directional antennas in both the base station and user equipment (UE) than is practical at lower frequencies. Antenna arrays for which the radiation pattern can be steered are particularly interesting because higher gain in the desired direction makes up for some of the added path loss, and the narrower beamwidth can reduce same-cell interference. At mmWave, arrays become more practical, even for a mobile phone.<sup>2</sup>

A significant metric for the performance of a mobile phone antenna is the gain in the direction of the base station. Since the orientation of a phone and direction toward the tower can vary greatly, the phone should be able to point its maximum gain in any direction. Hence, characterizing the ability of an antenna system to accomplish this is an important metric; one way to do this is predicting or measuring the effective or equivalent isotropic radiated power (EIRP) over all possible directions.

## EIRP AND CDF

EIRP, which is a function of direction, is the gain of a transmitting antenna in that direction multiplied by the power delivered to the antenna from the transmitter.<sup>3</sup> EIRP can be thought of as the equivalent power required to be delivered to an isotropic antenna to produce the same signal level. For example, if an antenna is driven by 2 mW (3 dBm) from the transmitter and the antenna has 5 dB gain in a given direction, the EIRP in that direction is 8 dBm; the signal in that direction would be the same as if the antenna were isotropic and driven with an 8 dBm signal.

Antenna gain,  $G$ , and EIRP,  $E$ , are usually expressed as a function of direction, i.e.,  $G(\theta, \varphi)$  and  $E(\theta, \varphi)$ . For practical antennas, gain and EIRP are typically continuous functions with minimum and maximum values:

$$\begin{aligned} 0 < G_{\min} < G_{\max} < \infty \text{ and} \\ 0 < E_{\min} < E_{\max} < \infty \end{aligned} \quad (1)$$

In dB,

$$\begin{aligned} -\infty < G_{\min} < G_{\max} < \infty \text{ and} \\ -\infty < E_{\min} < E_{\max} < \infty \end{aligned} \quad (2)$$

For an ideal isotropic antenna,  $G_{\min} = G_{\max}$  and  $E_{\min} = E_{\max}$ .

We can define a probability density function,  $f(E(\theta, \varphi))$ , over all directions ( $0 \leq \theta \leq \pi$ ,  $0 \leq \varphi < 2\pi$ ) as

$$\int_{-\infty}^{\infty} f(E)dE = \int_{E_{\min}}^{E_{\max}} f(E)dE = 1 \quad (3)$$

The probability over all directions of the EIRP being between any two values  $E_1$  and  $E_2$  (inclusive) is

$$P = \int_{E_1}^{E_2} f(E)dE \quad (4)$$

In a typical polar 3D gain or EIRP plot, the magnitude at each  $\theta$  and  $\varphi$  is plotted as a radius from the origin. For this type of plot, the EIRP of an antenna system will be contained in the closed region between a sphere of radius  $E_{\min}$  centered on the origin and an equal or larger sphere centered on the origin of radius  $E_{\max}$ .

A cumulative distribution function (CDF) or, simply, the distribution function of the probability density function  $f(x)$  is

$$F(x_1) = \int_{-\infty}^{x_1} f(x)dx \quad (5)$$

and gives the probability that  $x \leq x_1$ .<sup>4</sup>

For the EIRP probability density function  $f(E)$ , the corresponding CDF,  $F_E(x)$ , gives the probability that the EIRP will be  $\leq x$ :

$$F_E(x < E_{\min}) = 0 \text{ and } F_E(x \geq E_{\max}) = 1 \quad (6)$$

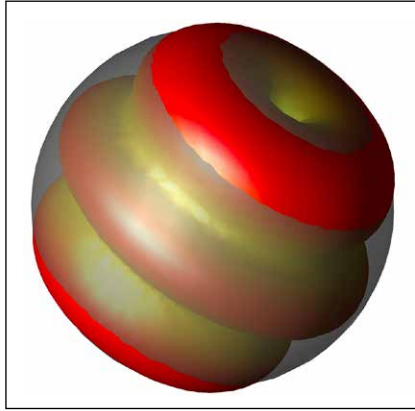
For  $E_{\min} \leq x \leq E_{\max}$ ,  $F_E(x)$  gives the fraction of all possible directions (i.e., fraction of  $4\pi$  steradians) for which  $E \leq x$  and  $(1 - F_E)$  gives the fraction for which  $E > x$ , i.e., the fraction of a polar plot of  $E$  which is "poking out" of a sphere of radius  $x$ . For example, **Figure 1** shows a sphere representing the realized gain of the  $3\lambda/2$  resonance of a 76 mm printed circuit dipole, showing a magnitude of 2 dBi. Approximately 10 percent of the directions have gain more than 2 dBi; in this case,  $F(2 \text{ dBi}) \cong 0.9$ , so about 90 percent of the gain pattern is contained within the sphere.

When the EIRP over the sphere is sampled at a finite number of directions, such as in a measurement or simulation, the CDF can be approximated by

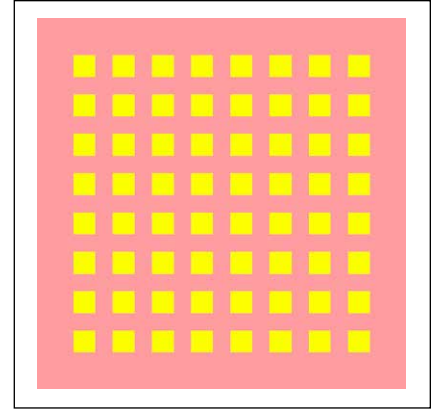
$$F_E(x) \cong \frac{\# \text{Directions with } E \leq x}{\text{Total } \# \text{ of Directions}} \quad (7)$$

## PATCH ARRAY

To illustrate, the CDF of the EIRP will be calculated for a 64 element patch array antenna at 28 GHz.<sup>5</sup> All simulations and processing are performed using XFDTD®.<sup>6</sup> The geometry is an  $8 \times 8$  element patch array on a 52.5 mm  $\times$  52.5 mm  $\times$  0.254 mm substrate with a ground plane (see **Figure 2**). The electrical parameters of the substrate are  $\epsilon_r = 2.2$  and loss tangent = 0.0009. This example is restricted to the antenna array structure to illustrate the method. In practice, the antenna would



▲ Fig. 1 Realized gain CDF at the  $3\lambda/2$  resonance of a 76 mm printed circuit dipole.

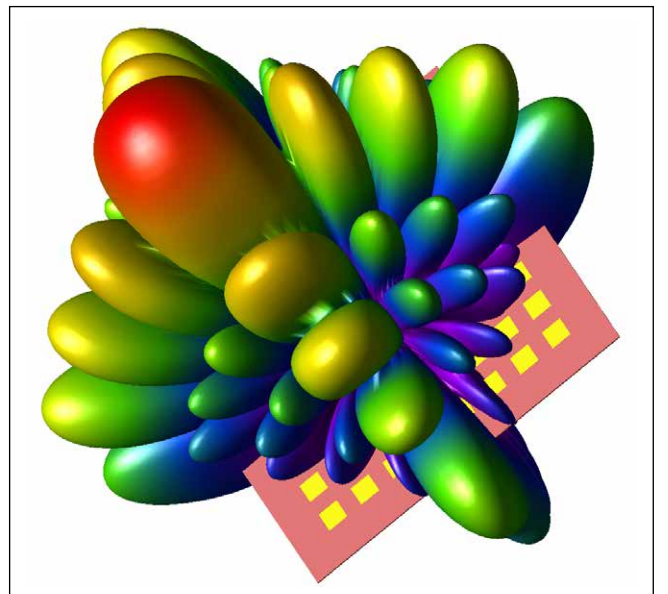


▲ Fig. 2  $8 \times 8$  patch antenna array on a 52.5 mm  $\times$  52.5 mm substrate.

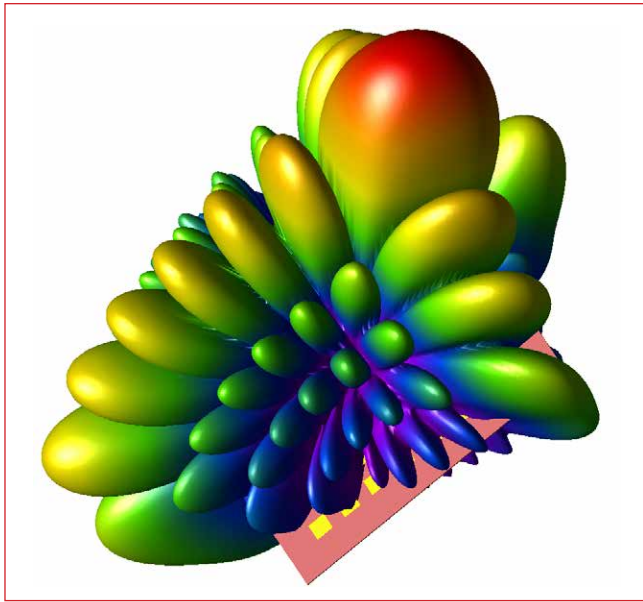
be evaluated by itself in the initial stages of the design, then simulated in a more complex environment, including the complete mobile phone geometry and, possibly, other arrays added for better diversity of coverage and polarization.

The realized gain patterns for maximum signal in two directions are shown in **Figures 3** and **4**. Figure 3 shows the radiation pattern of the array with all elements fed in phase, so the principal lobe is perpendicular to the plane of the antenna, i.e.,  $\theta = 90$  degrees. The maximum gain is 24.2 dBi. Figure 4 shows the radiation pattern of the array with all elements fed with a phase taper across the 2D array, so the principle lobe is along the direction  $\theta = 37$  degrees and  $\theta = 90$  degrees. The maximum realized gain in this case is 23 dBi. A single element of this array will have reduced gain toward the back (i.e., the ground plane side), so the array will not have gain as high in that hemisphere. Also, integrating the array into a phone will yield additional effects on the radiation pattern.

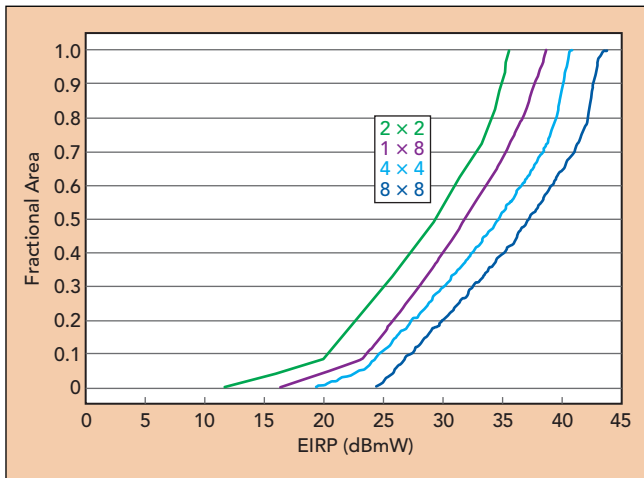
Determining how well the array performs in every direction is useful. What is the distribution of EIRP over the sphere? Since this is a simulation, it is straightforward



▲ Fig. 3 Realized gain of the  $8 \times 8$  patch, fed for maximum gain normal to the plane of the patches.



▲ Fig. 4 Realized gain of the  $8 \times 8$  patch, fed for maximum gain at  $\theta = 37$  degrees and  $\varphi = 90$  degrees.



▲ Fig. 5 EIRP CDFs for the full  $8 \times 8$  element patch array and several subarrays.

to characterize the maximum gain in many directions. However, to capture the many variations we expect on the gain pattern due to the geometry, the number of sample directions needs to be large. The CDF of EIRP provides a useful, one-dimensional function to characterize the array's performance over all possible directions.

The far zone radiation due to each element in the array is computed for the full geometry. These patterns can be combined in post processing to compute the gain and EIRP for any combination of elements, enabling the power and phase delivered to each element to be set independently. To compute the CDF, the phase of each element in the array is adjusted to provide maximum EIRP in each of a suitably large number of sample directions representing the sphere of all possible directions. The CDF of EIRP function can then be computed from Equation 7.

A CDF of the EIRP for the full  $8 \times 8$  element array and several subarray combinations is shown in **Figure 5**. For all cases, the transmitter is assumed to have a power

of 23 dBm, which is typical for a mobile phone. For the  $8 \times 8$  element case, the EIRP is about 37 dBm at a fractional area of 0.5, which means that half of the directions have an EIRP larger than 37 dBm. For the  $4 \times 4$  subarray, elements from one quarter of the array are used to determine the CDF of EIRP. This CDF curve has a similar shape but shifted down in EIRP, as expected for an array with one quarter as many elements. Elements from one corner of the array are used in the CDF for the  $2 \times 2$  subarray, and the CDF has a similar drop in EIRP compared to the  $4 \times 4$  case. Finally, a  $1 \times 8$  arrangement of elements from one side of the array shows the EIRP lies between the  $2 \times 2$  and  $4 \times 4$  element subarrays, again as expected. This type of array might be used in a mobile phone, with arrays on two sides to provide more complete coverage.

As seen from these curves, about half of the possible directions have significantly lower EIRP due to the ground plane, which emulates the placement of the array in a phone. One way to provide broader coverage is to place multiple antenna arrays in the device, such as on either edge of the mobile phone, as mentioned. By properly combining the distributions, the CDF of the EIRP can be used to estimate the ability of multiple arrays or subarrays to work in combination to provide higher EIRP in all directions and reduce blind spots. This measure can also be evaluated using multiple antennas for diversity and coverage in all polarizations.

## CONCLUSION

Steerable array antennas are of significant interest to help meet the goals of 5G mobile communications. At mmWave frequencies, such as 28 and 38 GHz, fairly large and directional arrays become practical for relatively small devices such as mobile phones; however, these frequencies have higher path loss than at microwave frequencies which have been used in previous generations. For a given power level, the ability of antenna arrays to control the direction of maximum radiation will allow for much better EIRP in the direction of communications.

The CDF of EIRP, computed from a suitably large number of sample directions, may be used to assess the directionality and effective coverage of an antenna array. The article used a simple example of an  $8 \times 8$  patch antenna array to demonstrate the usefulness of the CDF of EIRP to characterize the ability of an array to provide good EIRP in all directions. ■

## References

1. T. S. Rappaport, S. Sun, R. Mayzus, H. Zhao, Y. Azar, K. Wang, G. N. Wong, J. K. Schulz, M. Samimi and F. Gutierrez, "Millimeter Wave Mobile Communications for 5G Cellular: It Will Work!," *IEEE Access*, 2013, pp. 1:335–349.
2. W. Hong, K. Baek and S. Ko, "Millimeter-Wave 5G Antennas for Smart-Phones: Overview and Experimental Demonstration," *IEEE Transactions on Antennas and Propagation*, Vol. 65, No. 12, December 2017, pp. 6250–6261.
3. "Definitions of Terms for Antennas," *IEEE Standard 145-2013*, 2013.
4. W. Feller, "An Introduction to Probability Theory and Its Applications, Volume I," *John Wiley & Sons Inc.*, 1959, p. 168.
5. Remcom, "Beamforming for an  $8 \times 8$  Planar Phased Patch Antenna Array for 5G at 28 GHz," *Microwave Journal*, January 11, 2019, [www.microwavejournal.com/articles/31634](http://www.microwavejournal.com/articles/31634).
6. "Xfdtd," *Remcom Inc.*, March 2019.

# Characterizing Circuit Materials at mmWave Frequencies: Part I

John Coonrod  
Rogers Corp., Chandler, Ariz.

*Different dielectric constant measurement methods provide different results.*

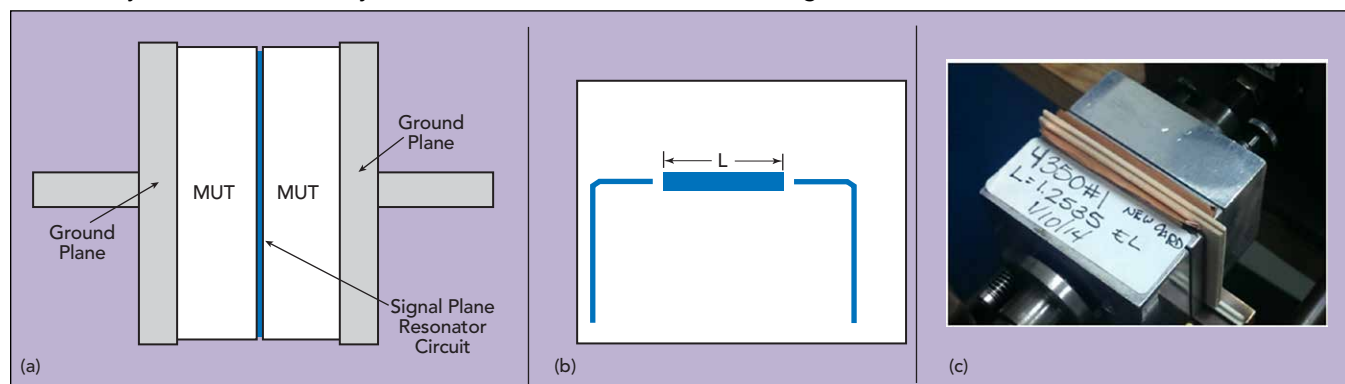
The dielectric constant (Dk) or relative permittivity of a circuit material is not a constant—despite what its name might imply. The Dk of a printed circuit board (PCB) material, for example, will change as a function of frequency. Also, using different Dk test methods on the same piece of material, they are likely to measure different Dk values, which are correct for those test methods. As circuit materials are increasingly employed at mmWave frequencies, with the growth of 5G and advanced driver assistance systems, it is important to understand how Dk changes with frequency and which Dk test methods are “best” applied.

No industry-standard best test method exists for measuring circuit material Dk at mmWave frequencies, although organizations such as the IEEE and IPC have committees devoted to this topic. It is not the lack of measurement methods; in fact, more than 80 are described in just one reference by Chen et al.<sup>1</sup> No method

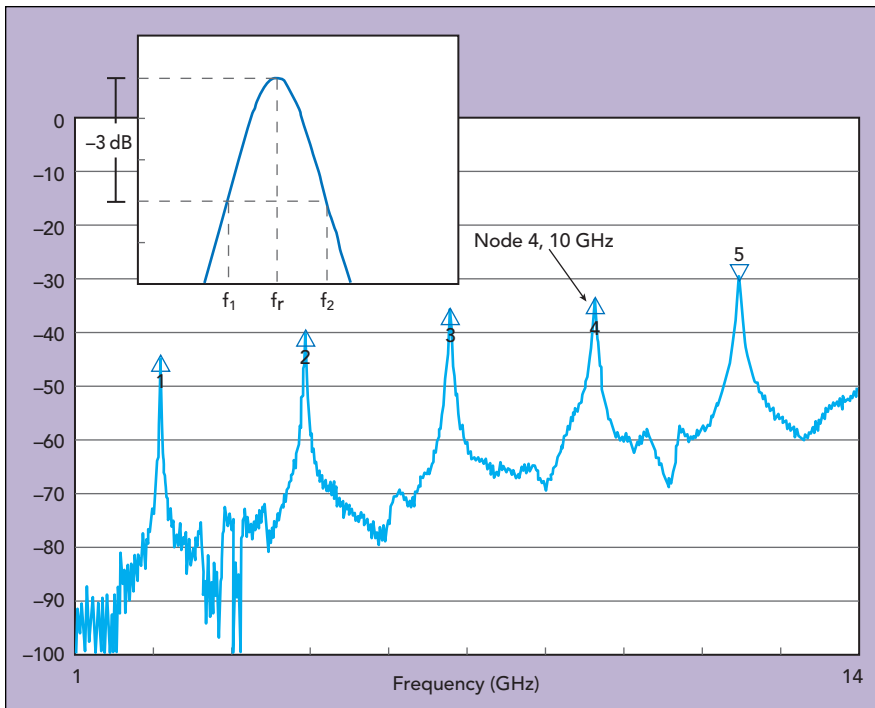
is ideal, with each having challenges and shortcomings, especially at frequencies from 30 to 300 GHz.

## CIRCUIT vs. RAW MATERIAL TESTS

Tests for determining circuit material Dk or Df (the loss tangent or  $\tan\delta$ ) are generally performed in one of two ways: either on the raw material or a circuit fabricated from the material. Raw material tests depend on high quality test fixtures and test equipment to extract Dk and Df values directly from the material. Circuit tests use a common circuit and extract the material parameters from the circuit’s performance, such as measuring the center frequency or frequency response of a resonator. Raw material tests introduce uncertainties typically associated with the test fixture or test setup, while circuit tests contain uncertainties from the test circuit design and fabrication techniques. Because the two methods differ, measurement results and accuracy levels typically do not agree.



▲ Fig. 1 X-Band clamped stripline test fixture side view (a), stripline resonator (b) and photograph (c).



▲ Fig. 2 Wideband clamped stripline measurement of a MUT 60 mils thick, with a  $D_k = 3.48$ .

For example, an X-Band clamped stripline test defined by IPC,<sup>2</sup> a raw material test, may not provide  $D_k$  results agreeing with a circuit test of the same material. The raw material test creates a stripline resonator by clamping two pieces of the material under test (MUT) in a special test fixture. Air can become entrapped between the MUT and the thin resonator circuit which is part of the fixture. The air becomes part of the measurement and lowers the measured  $D_k$ . If a circuit test is performed on the same circuit material, without the entrapped air, the measured  $D_k$  will be different. For a high frequency circuit material with a  $D_k$  tolerance of  $\pm 0.050$  determined from a raw material test, a tolerance of  $\pm 0.075$  may result from a circuit test.

Circuit materials are anisotropic, often with different  $D_k$  values in the three material axes.  $D_k$  values typically differ little between the x- and y-axis, so for most high frequency materials,  $D_k$  anisotropy comparisons are usually made between the z-axis and the x-y plane. For the same MUT, test methods that measure  $D_k$  for the z-axis can provide different results than test methods used to evaluate  $D_k$  in the x-y plane, although the values of  $D_k$  may be “correct” for the given method.

The type of circuit used for a circuit test also influences the value of the measured  $D_k$ . In general, two types of test circuits are used: resonant structures and transmission/reflection structures. Resonant structures typically provide narrowband results, while transmission/reflection tests are usually wideband. Methods using resonant structures are typically more accurate.

## TEST METHOD EXAMPLES

An example of a raw material test is the X-Band clamped stripline method. It has been used by manufacturers of high frequency circuit laminates for years and

is a dependable means of determining the  $D_k$  and  $D_f$  ( $\tan\delta$ ) in the z-axis of a circuit material. It uses a clamping fixture to form a loosely coupled stripline resonator from MUT samples. The measured quality factor ( $Q$ ) of the resonator is the unloaded  $Q$ , so it can be measured with minimal impact from cables, connectors and fixture calibration. The MUT is a copper-clad circuit laminate with all the copper etched from the substrate prior to testing. The raw circuit material is environmentally conditioned, cut to size and placed into the fixture on both sides of the resonator circuit at the signal plane (see Figure 1).

The resonators are designed with half-wavelength resonances starting at about 2.5 GHz, so node 4 is around 10 GHz; this is the node commonly used for  $D_k$  and  $D_f$  measurements. Lower nodes and frequencies can be used—even the higher node 5 can be used, although higher nodes are usually avoided due to wave propagation or measurement issues from harmonics and spurious content. The extraction of the  $D_k$  or relative permittivity ( $\epsilon_r$ ) is straightforward:

$$\epsilon_r = \left[ \frac{nc}{2f_r(L + \Delta L)} \right]^2 \quad (1)$$

where  $n$  is the node,  $c$  is the speed of light in free space and  $f_r$  is the center frequency of the resonant peak.  $\Delta L$  compensates for the electrical length extension due to electric fields in the gap-coupled area. Extraction of  $\tan\delta$  ( $D_f$ ) from the measurements is also straightforward. It is a fraction related to the 3 dB bandwidth of the resonant peak after subtracting the conductor losses ( $1/Q_c$ ) associated with the resonator circuit.

$$\frac{1}{Q_u} = \frac{1}{Q_c} + \frac{1}{Q_d} \quad (2)$$

$$\tan\delta \propto \frac{1}{Q_d} \quad (3)$$

$$\tan\delta = \left[ \frac{f_2 - f_1}{f_r} \right] - \frac{1}{Q_c} \quad (4)$$

Figure 2 shows a measurement using the clamped stripline test method with a 60-mil thick MUT with  $D_k = 3.48$ .

Ring resonators are often used as test circuits.<sup>3</sup> They are simple microstrip structures having resonances at integer multiples of the mean circumference of the microstrip ring (see Figure 3a). They are typically loosely coupled, as loose coupling between the feed lines and the ring minimizes the capacitance of the gaps between the feed lines and the ring. This capacitance changes with frequency, causing the resonant frequency to shift

and resulting in errors when extracting the material Dk. The conductor width of the resonator ring should be much smaller than the radius of the ring —as a rule of thumb, one-quarter the dimension of the ring radius or smaller.

The  $|S_{21}|$  response of a microstrip ring resonator on a 10-mil thick circuit material with  $Dk = 3.48$  is shown in **Figure 3b**. An approximate calculation of the Dk is given by

$$2\pi r = n\lambda_g \quad (5)$$

$$\lambda_g = \frac{c}{f\sqrt{Dk_{\text{eff}}}} \quad (6)$$

$$Dk_{\text{eff}} = \left[ \frac{cn}{2\pi rf} \right]^2 \quad (7)$$

Although approximate, these formulas are useful for determining an initial Dk value. A more accurate Dk can be found using an electromagnetic (EM) field solver and precise resonator circuit dimensions.

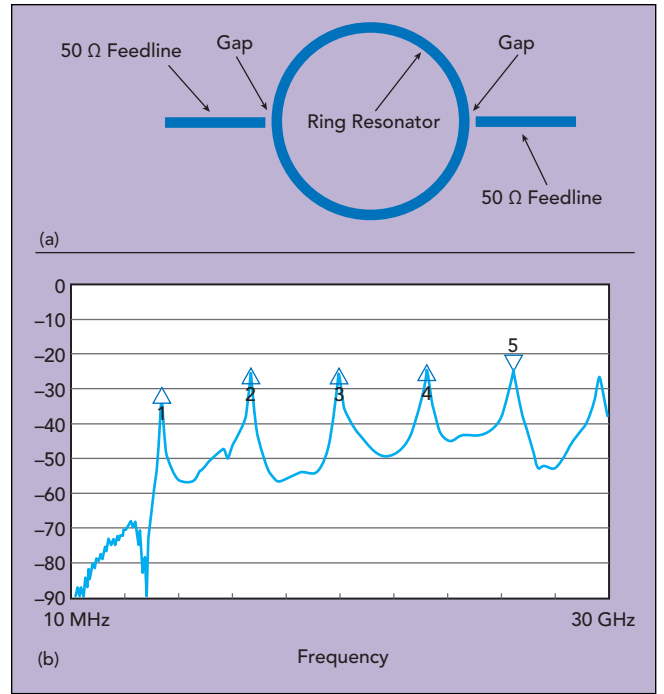
Loosely coupled resonators are often used for Dk and Df measurements to minimize resonator loading effects. Coupling should be loose enough so the insertion loss is 20 dB or less at the resonant peak. In some cases, with extremely weak coupling, the resonant peak may be so weak that it cannot be measured. This typically occurs for resonant circuits with thinner substrates, the types of materials commonly used in mmWave applications, since the high frequencies have small wavelengths and circuit dimensions.

### mmWAVE TEST METHODS

While there are many Dk test methods, only some are suitable for mmWave frequencies, yet none are accepted as industry standards. However, the following methods are accurate and repeatable at mmWave.

#### Differential Phase Length Method

The microstrip differential phase length method has been used for many years.<sup>4</sup> It is a transmission test method in which phase measurements are made on two circuits that only differ by physical length (see **Figure 4**). To avoid any variations in circuit material properties, the circuits are fabricated side-by-side and as close together as possible on the MUT. The circuits are 50  $\Omega$  microstrip transmission lines of different lengths with a grounded coplanar waveguide (GCPW) signal launch. At mmWave frequencies, the GCPW signal launch is important, since the launch area can have a major impact on return loss. End-launch connectors should also be used, to make good pressure contacts between the coaxial connectors and the test circuit without soldering, allowing the same two connectors to be used for the shorter and longer circuits. This minimizes the effect of the connectors on measurement results. For consistency, the same connectors should be oriented to the same ports of the vector network analyzer (VNA). If connector A is oriented to port 1 of the VNA and connector B to port 2 for testing the shorter circuit, the same should be true



**▲ Fig. 3 Microstrip ring resonator (a) and wideband measurement (b).**

when testing the longer circuit.

Subtracting the phase angles of the short and long circuits will also subtract the effects of the connectors and the signal launch areas. If the return loss is good for both circuits and the connectors have consistent orientation, most of the effects of the connectors will be minimized. When using this method at mmWave frequencies, return loss at these transitions of better than 15 dB through 60 GHz and 12 dB from 60 to 110 GHz is considered acceptable.

The extraction equations for the microstrip differential phase length method are based on a manipulation of the microstrip phase response formula for circuits with different physical lengths:

$$\Phi = 2\pi f \frac{\sqrt{\text{Eff} - \epsilon_r} L}{c} \quad (8) \quad \text{where } c \text{ is the}$$

$$\Delta\Phi = 2\pi f \frac{\sqrt{\text{Eff} - \epsilon_r}}{c} \Delta L \quad (9)$$

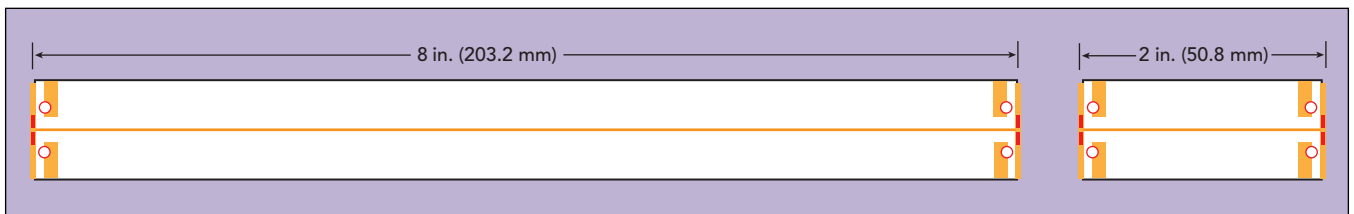
$$\text{Eff} - \epsilon_r = \left[ \frac{\Delta\Phi c}{2\pi f \Delta L} \right]^2 \quad (10)$$

speed of light in free space,  $f$  is the frequency of the  $S_{21}$  phase angle,  $\Delta L$  is the difference in physical lengths of the two circuits and  $\Delta\Phi$  is the difference in phase angle between the shorter and longer circuits.

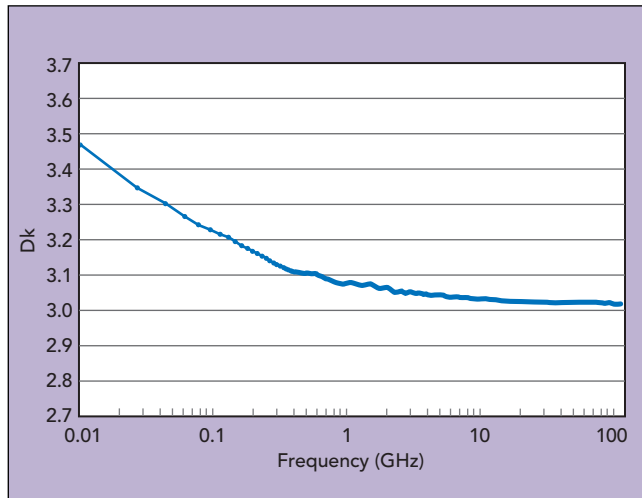
The test method comprises a few simple steps:

- Measure the  $S_{21}$  phase angle as a function of frequency for the shorter and longer circuits.
- Use the formulas to determine the measured effective Dk.
- Obtain precise and accurate circuit dimensions that can be entered into an EM field solver using the initial Dk value for the material.

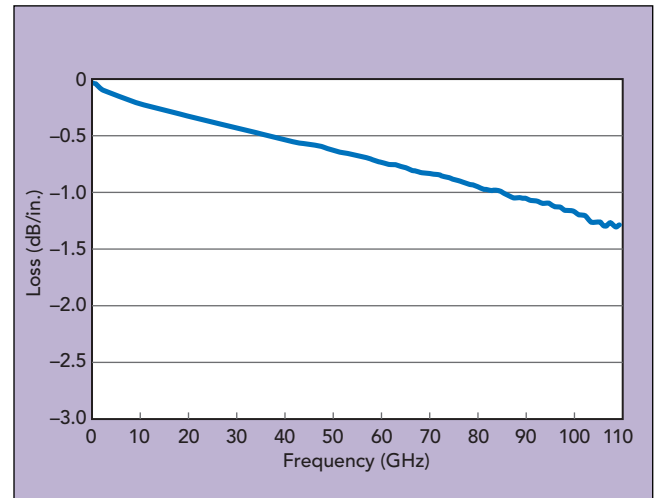




▲ Fig. 4 Top view of the long and short microstrip circuits used in the differential phase-length method.



▲ Fig. 5 Dk vs. frequency measured with the microstrip differential phase length method.



▲ Fig. 6 Insertion loss vs. frequency determined from the microstrip differential length measurements.

- Use the software to generate a simulated effective Dk value. Change the Dk in the solver until the measured and simulated effective Dk values for the material match at the same frequency.
- By incrementing the frequency into the mmWave region and repeating this process, the Dk value can be determined across a range of frequencies through mmWave.

**Figure 5** shows a measurement using the microstrip differential phase length method with 5-mil thick RO3003G2™ circuit material. The curve was generated using a Microsoft Windows PC program developed by Rogers Corp.<sup>5</sup> The data reflects the usual trend of decreasing Dk with increasing frequency. At lower frequencies, larger changes in Dk occur versus frequency; however, from 10 to 110 GHz, the Dk shows little change. This curve reflects a material with low loss and rolled copper with a smooth surface. A material with high loss and/or higher copper surface roughness will exhibit an increased negative slope in the Dk-frequency relationship. Using this test method, the insertion loss for circuits using the MUT can be obtained by subtracting the  $S_{21}$  values of the shorter and longer circuits at each frequency (see **Figure 6**).

### Ring Resonator Method

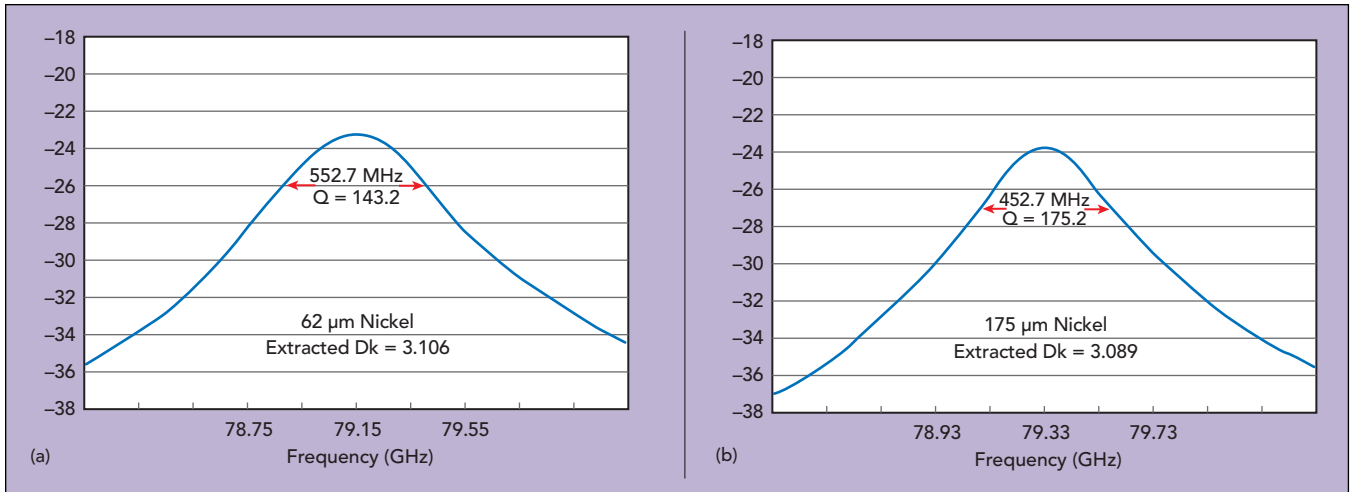
The ring resonator method is another approach for mmWave characterization. While ring resonators are often used below 10 GHz, with proper fabrication precision they can be used effectively at mmWave frequencies. Fabrication is important because the effects of circuit dimensions and dimensional tolerances are greater at mmWave, with any variation reducing accuracy. The thickness of the copper plating on the circuit material

also varies, as does the gap dimension. Most mmWave ring resonators are thin (usually 5 mils), and the gap between the feed line and resonator ring is also small. Thickness and gap variations for a gap-coupled ring resonator will impact both coupling and the resonant frequency.

When comparing two circuits built on the same circuit material and with different copper plating thicknesses, the circuit with the thicker copper will exhibit a lower Dk. The resonant frequencies of the two circuits will also differ, even though they should be the same for the same circuit material and test method. **Figure 7** shows an example where the thickness variation in a circuit's final plated finish causes differences in the extracted Dk for the same material. Whether the finish is electroless nickel immersion gold (ENIG) or other plated finishes, the issue remains.

Besides these fabrication issues, conductor width variation, etched-space variation, trapezoidal effects and substrate thickness variation cause similar effects. If all these variations are accounted for, one individual ring resonator measurement can yield the correct Dk value; however, many test routines will assume nominal circuit dimensions and extract an incorrect Dk. At lower frequencies these effects do not impact Dk accuracy as much as at mmWave frequencies.

Another significant variable using ring resonators at mmWave is the gap coupling changing with frequency. It is typical for ring resonators to be evaluated using multiple nodes, with the nodes usually spaced by significant differences in frequency. As a result, gap coupling variation can be a significant source of error. To overcome this, a differential circumference method is used. This approach uses two ring resonators, essentially identical



▲ Fig. 7 mmWave ring resonator measurements of a MUT with 62 μm thick (a) and 175 μm thick (b) nickel plating.

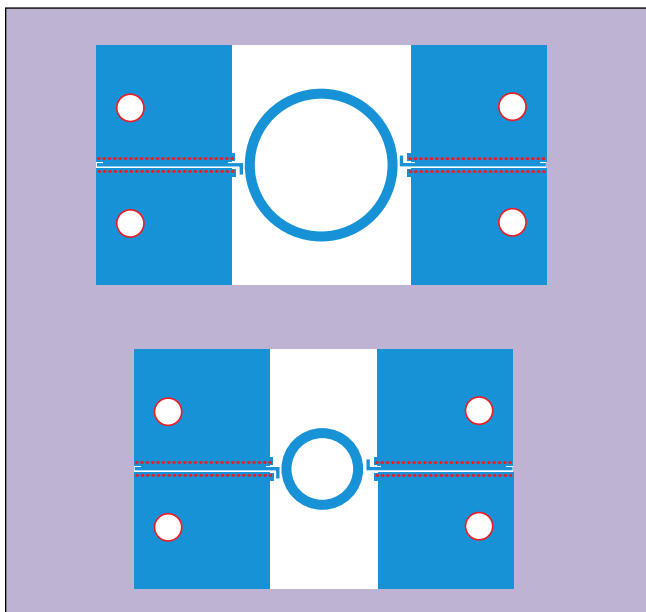
except the ring circumferences differ in size and are integer multiples of each other (see **Figure 8**). With two ring resonators, the higher order resonant nodes used in the Dk extraction have some frequencies in common. Since the feed lines and gaps are the same, the effects of gap coupling are decreased—theoretically eliminated—which leads to better accuracy in the extracted Dk. The Dk is calculated from the equations:

$$L_1 + \Delta L = \frac{n_1 c}{2f_{r1} \sqrt{\text{Eff}_{-}\epsilon_r}} \quad (11)$$

$$L_2 + \Delta L = \frac{n_2 c}{2f_{r2} \sqrt{\text{Eff}_{-}\epsilon_r}} \quad (12)$$

$$\text{Eff}_{-}\epsilon_r = \left[ \frac{c(n_1 f_{r2} - n_2 f_{r1})}{2f_{r1} f_{r2} (L_2 - L_1)} \right]^2 \quad (13)$$

The ring resonators in Figure 8 are microstrip structures, with the feed lines tightly-coupled GCPW to avoid open-end feed line resonances, which could in-



▲ Fig. 8 Test rings used with the microstrip differential circumference ring resonator method.

terfere with the ring resonant peaks. If the feed lines were open-ended microstrip, they would have their own resonances. The only way to avoid this is to make the feed lines much shorter or use tightly-coupled GCPW feed lines. Since the differential circumference ring resonator method yields the circuit's effective Dk, it is still necessary to make accurate circuit dimension measurements and use a field solver to extract the material Dk.

## CONCLUSION

The mmWave test methods discussed here are circuit-based. Several other methods may be considered, such as raw material tests, but most yield a material Dk for the x-y plane rather than the z-axis (thickness). Circuit designers are more interested in the z-axis Dk, but for those willing to work with x-y material Dk values, free-space measurements, split-cylinder resonator measurements and waveguide perturbation testing are additional test methods.

The clamped broadside coupled stripline resonator test method has also been evaluated for determining circuit material Dk at mmWave frequencies. Unfortunately, this approach is most effective with small pieces of MUT and is not practical for volume testing. The quest continues to find a good raw material test to characterize materials at mmWave frequencies. ■

## References

1. L. F. Chen, C. K. Ong and C. P. Neo, "Microwave Electronics, Measurement and Material Characterization," John Wiley & Sons Ltd., 2004.
2. IPC-TM-650 Test Method Manual, "Stripline Test for Permittivity and Loss Tangent (Dielectric Constant and Dissipation Factor) at X-Band," IPC, March 1998, pp. 1–25.
3. K. Chang and L. H. Hsieh, "Microwave Ring Circuits and Related Structures," Wiley-Interscience, division of John Wiley & Sons, New York, 2004.
4. N. K. Das, S. M. Voda and D. M. Pozar, "Two Methods for the Measurement of Substrate Dielectric Constant," *IEEE Transactions on Microwave Theory and Techniques*, Vol. 35, No. 7, July 1987, pp. 636–642.
5. "ROG Dk Calculator," Rogers Corp. Technology Support Hub. [www.rogerscorp.com/acs/technology/index.aspx](http://www.rogerscorp.com/acs/technology/index.aspx).

# Characterizing Circuit Materials at mmWave Frequencies: Part II

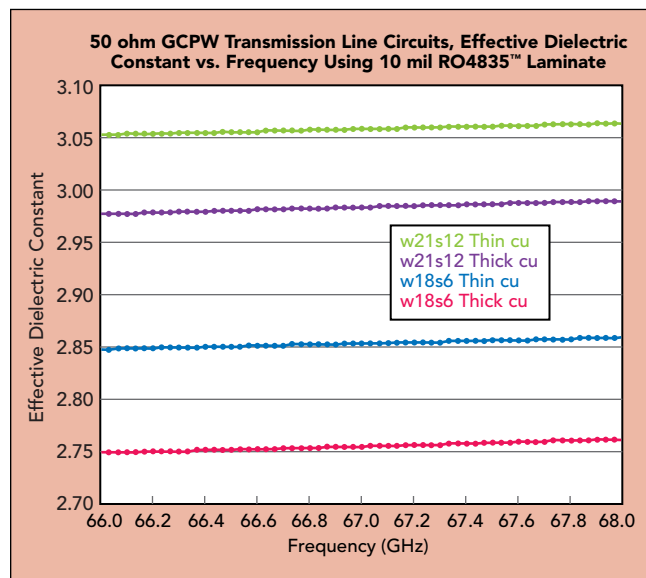
John Coonrod  
Rogers Corp., Chandler, Ariz.

*Different Dk measurement methods can provide different test results, depending upon the many variables involved.*

The first part of this article (See page 14 in this ebook) explored several methods for measuring the dielectric constant (Dk) or relative permittivity of a circuit material at mmWave frequencies, including by means of ring resonators. Part 2 will take a closer look at ring resonators and how they can be used to determine the Dk and the loss tangent (Df) of a high frequency printed circuit board (PCB) material. The importance of characterizing circuit material properties at higher frequencies increases steadily as interest grows in potentially large applications at mmWave frequencies, including automotive radar and 5G wireless communications.

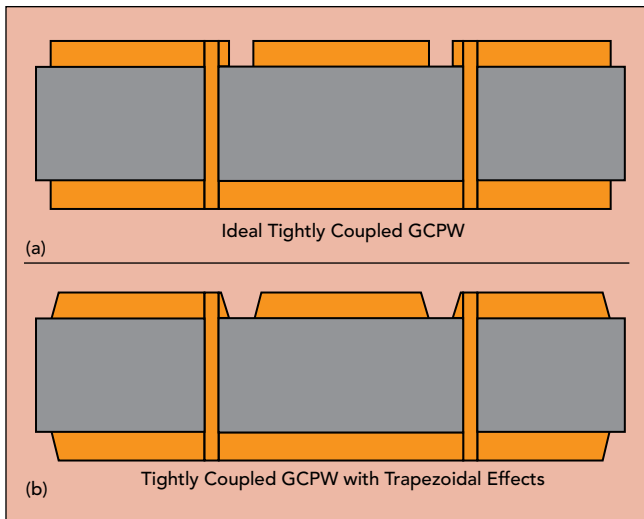
Ring resonators are often used to determine the Dk and Df of high frequency circuit materials. While they are typically used to characterize materials at frequencies less than 12 GHz, they can be used at higher frequencies provided that several issues are addressed. One of these concerns is the RF/microwave performance variations that occur in a ring resonator as a result of normal process variations that can impact the fabrication and construction of the resonator PCB, such as variations in the thickness of the PCB's copper plating.

Electrical connections between different conductor layers of PCBs are typically made by plated thru hole (PTH) vias formed through the z axis (thickness) of the circuit material. Conductive paths through the vias are formed with electroless copper plating and then final electrolytic copper plating. Copper plating is also performed on the outer conductive layers of the PCB, increasing the thickness of the copper supplied with the circuit laminate material. The plating process is subject to normal variations in copper plating thickness.

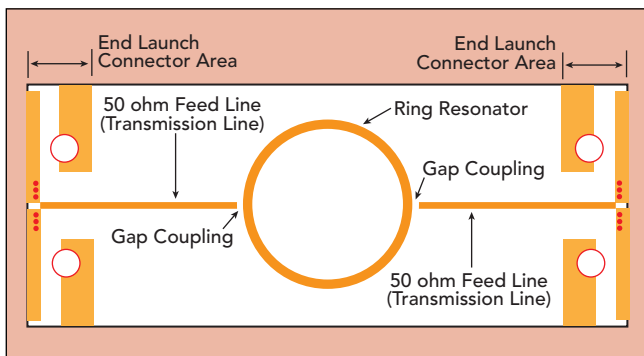


▲ Fig. 1 Excerpt from article [1] showing effective dielectric constant versus frequency for the four groups of GCPW, with tight coupling (s6), loose coupled (s12), and thin and thick copper.

Depending on frequency and design, the performance of some circuits can be impacted by these variations in copper plating thickness. Normally, circuits formed with microstrip transmission lines will not be affected. But coupled circuits and circuits with different transmission-line technologies, such as grounded coplanar waveguide (GCPW), can exhibit performance variations as a result of variations in the PCB copper thickness. A good example of this was published previously (see Figure 1).<sup>1</sup>



▲ Fig. 2 Cross-sectional views of GCPW circuits with ideal, rectangular shaped conductors (a) and trapezoidal-shaped conductors (b).



▲ Fig. 3 Description of a microstrip ring resonator circuit.

The naming convention for the effective Dk curves of the GCPW circuits in Figure 1 refer to the signal conductor width ( $w$ ) and the space ( $s$ ) between the signal conductor and the neighboring coplanar ground planes. The curve for  $w18s6$  refers to a circuit with an 18-mil-wide signal conductor and space or gap between both sides of the signal conductor and the neighboring ground planes that is 6 mils wide. All circuits in this study were built on the same panel of circuit material to minimize material variations which could impact measurement results.

As can be seen in Figure 1, there is an approximate difference of 0.1 in the values of effective Dk determined when using the same design ( $w18s6$ ) for circuits with thin copper (about 1 mil thick) compared to circuits with thick copper (about 3 mils thick). This design ( $w18s6$ ) is considered tightly coupled: the gap between the signal plane and neighboring coplanar ground planes is relatively small. As Figure 1 also shows, the loosely coupled design ( $w21s12$ ) was less impacted by the difference in copper thickness, with a difference of about 0.075 in effective Dk for circuits with thin and thick copper.

As shown in **Figure 2**, another concern with PCB copper thickness variations is related variations of trapezoidal effects.

Most electromagnetic (EM) simulation software will assume rectangular-shaped conductors for a GCPW circuit

(see Figure 2a). But a cross-sectional view of a GCPW circuit would show that most of the conductors will vary between rectangular and trapezoidal shapes (see Figure 2b). Depending upon the PCB fabrication process, the trapezoidal shape could be inverted compared to what is shown in Figure 2b, being narrower at the base of the conductor, which is the interface between the PCB's copper conductor and dielectric substrate.

A typical consequence of thicker copper is to have conductors with more of a trapezoidal shape than a rectangular shape. Variations from rectangular to trapezoidal conductor shapes can impact the electrical performance of coupled circuits. For tightly coupled GCPW circuits, rectangular shaped conductors have significant current density along the sidewalls of the coupled conductors, with increased electric fields along the coupled area. When the conductor shape changes to trapezoidal, the current density changes, with increased current density near the base of the conductor and lower current density along the coupled sidewalls. This results in decreased electric fields in the air around the trapezoidal shaped conductors. Having more or less electric fields in air will impact the capacitance in gap coupled areas and alter the effective dielectric constant as determined from measurements of such circuits.

The formation of trapezoidal conductors and their effects on circuit performance cannot be predicted or included in a circuit simulation as a standard procedure. However, for troubleshooting or evaluating a circuit, a small section of that circuit can be analyzed to determine the impact of trapezoidal conductor effects. The results of the partial circuit analysis will then be available for use in an EM simulator to better predict the overall effects of variations in conductor shape on circuit performance.

Because they are coupled structures, ring resonators can be impacted by certain PCB fabrication variations; copper plating thickness and trapezoidal conductor effects are among the concerns related to PCB fabrication variations. Most ring resonators are gap coupled (see **Figure 3**).

Feedlines bring energy into and out of a ring resonator circuit (see Figure 3). The feedlines are gap coupled to the ring resonator and the gap coupling can impact the resonant frequency. The gap coupling is sensitive to PCB copper thickness variations. When the copper is thin, less of the electric fields will occupy the air around the conductors and more electric fields will be in the substrate; the distribution of the electric field impacts the capacitance in the gap area and can alter the frequency of the ring resonator circuit. When the same circuit design is fabricated with a PCB having thicker copper, more of the electric field is in air and the capacitance in the gap area and the center frequency of the resonator will change. Although the ring resonator design is the same, it can exhibit significant variations in resonant frequency due to normal variations in PCB copper thickness and trapezoidal conductor effects. Because the same ring resonator can yield different results depending upon copper thickness and trapezoidal conductor effects, it can also provide a range of Dk values (some incorrect) when used as a test circuit.

Coupling is a key part of any ring resonator design and variations in PCB copper thickness and conductor shapes will impact the performance of a ring resonator depending upon the amount of coupling in a design. The effects have more impact when the coupling is tight than when it is loose. As a rule, the coupling should be relatively loose to avoid the impact of copper thickness and trapezoidal shape variations. Additionally, when the ring is very loosely coupled, the resonator circuit will behave more like an unloaded resonator and the effects of the gaps, feedlines, connectors, and cables are less significant. The coupling should be loose enough to where the resonant peak amplitude is no greater than -20 dB.

Most mmWave circuits are fabricated on thin substrates. Thinner substrates help minimize radiation, dis-

persion, and spurious wave propagating modes. Fabricating a loosely coupled ring resonator on a thin substrate with a resonant peak that can be measured is very difficult. For a thin substrate, the differences between a gap coupled ring resonator that is loosely coupled compared to tightly coupled, at mmWave frequencies, can be a dimensional difference of less than 1 mil in the gap coupled area. Since most circuit fabricators can maintain an etching tolerance of at best  $\pm 0.5$  mil (a 1-mil variation), coupling variations for mmWave circuits can be significant from one circuit to the next when fabricating multiple circuits of the same design.

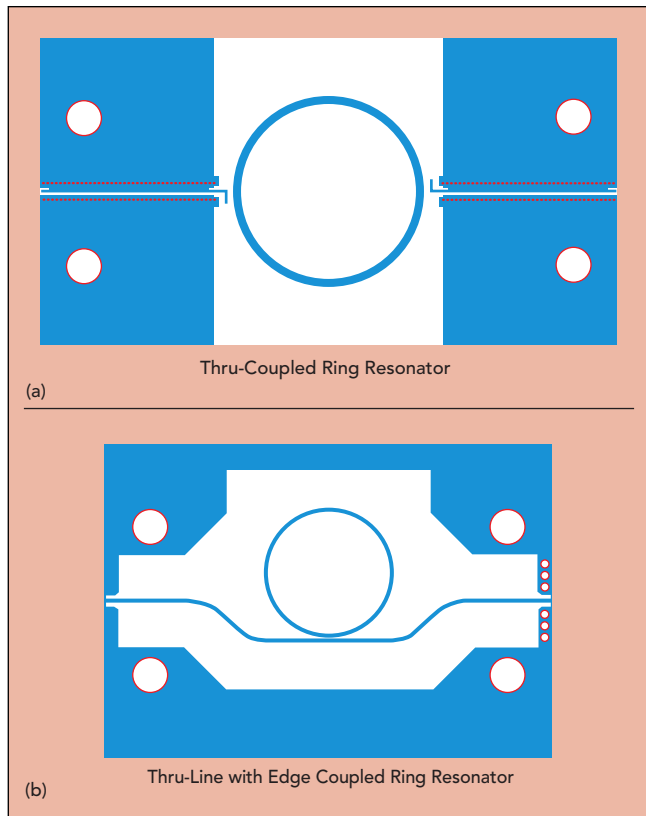
Not all ring resonator designs have the same sensitivity to gap coupling. For example, a thru-coupled ring resonator (see Figure 3) is sensitive to gap coupling variations but a thru-line design with an edge coupled ring resonator is less sensitive to gap coupling variations. Figure 4 provides illustrations of these two types of coupled resonators.

As was shown in Figure 8 of Part 1 of this article, feedlines for thin mmWave ring resonator circuits are best implemented in GCPW to prevent any open-ended feedline resonance which can interfere with the resonance of the ring. **Figure 4a** shows a thru-coupled ring resonator structure while Figure 4b depicts a thru-line edge coupled ring resonator. The thru-line transmission line in **Figure 4b** uses a GCPW structure in the end-launch connector area to optimize the signal launch. The signal launch is the transition from the connector to the PCB. It must be optimized for good return loss across the frequency range of interest for a ring resonator design.

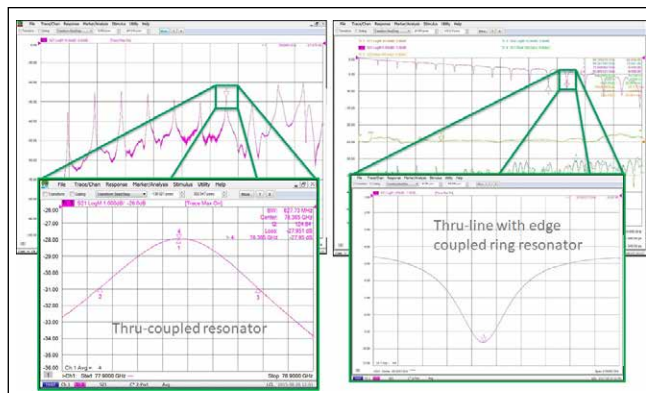
The thru-coupled ring resonator will exhibit resonant peaks as expected. However, the thru-line with ring resonator that is edge coupled will have a “suck-out” in measured amplitude-versus-frequency response at the frequencies where the ring resonates. The thru-line with edge-coupled ring resonator should have an S21 response much like that of a transmission line, although it will have periodic dips in its insertion loss versus frequency response where the ring resonates (see **Figure 5**).

**Table 1** provides a comparison to show potential differences in RF performance between these two different ring resonators due to normal variations in material properties and circuit fabrication processes.

Data in Table 1 is from models run in Sonnet Software,[2] a popular EM simulation software tool. The EM field solver has been shown to have excellent accuracy for planar circuits when simulation results are compared with measured results. The resonator models are based on 5-mil-thick RO3003™ circuit laminate with electrodeposited (ED) copper from Rogers Corp. The ring resonator designs were moderately coupled. The resonant peak for each resonator was tuned to -10 dB at the center frequency noted in Table 1. Several variations related to circuit material properties and PCB fabrication processes were modeled and the results are shown in Table 1. The description of most of the different models in the column headers is self-explanatory. However, the far right-hand column labeled “Narrow width, wider gap” shows the difference for a ring conductor with narrower width. With PCB fabrication and in a discrete circuit area



▲ Fig. 4 Illustrations of a thru-coupled ring resonator (a) and a thru-line edge coupled ring resonator (b).



▲ Fig. 5 Screen shots from a network analyzer show typical ring resonator performance for the thru-coupled ring resonator and the thru-line edge coupled ring resonator.

**TABLE 1****THRU-COUPLED RING RESONATOR**

	Baseline		10% Thinner Substrate		Thinner Copper		Thicker Copper		Narrow Width, Wider Gap	
	Inches	mm	Inches	mm	Inches	mm	Inches	mm	Inches	mm
Conductor Width	0.012	0.305	0.012	0.305	0.012	0.305	0.012	0.305	0.011	0.279
Coupling Gap	0.007	0.178	0.007	0.178	0.007	0.178	0.007	0.178	0.008	0.203
Substrate Thickness	0.005	0.127	0.0045	0.114	0.005	0.127	0.005	0.127	0.005	0.127
Copper Thickness	0.0015	0.038	0.0015	0.038	0.001	0.025	0.003	0.076	0.0015	0.038
Copper Roughness	0.00007874	0.0020	0.00007874	0.0020	0.00007874	0.0020	7.87E-05	0.0020	0.00007874	0.0020
Center Freq. (GHz)	77.41		77.52		77.52		76.96		77.44	
Dk from Freq. Shift	Reference		0.009		0.009		-0.035		0.004	

**THRU-LINE EDGE COUPLED RING RESONATOR**

	Baseline		10% Thinner Substrate		Thinner Copper		Thicker Copper		Narrow Width, Wider Gap	
	Inches	mm	Inches	mm	Inches	mm	Inches	mm	Inches	mm
Conductor Width	0.012	0.305	0.012	0.305	0.012	0.305	0.012	0.305	0.011	0.279
Coupling Gap	0.006	0.152	0.006	0.152	0.006	0.152	0.006	0.152	0.007	0.178
Substrate Thickness	0.005	0.127	0.0045	0.114	0.005	0.127	0.005	0.127	0.005	0.127
Copper Thickness	0.0015	0.038	0.0015	0.038	0.001	0.025	0.003	0.076	0.0015	0.038
Copper Roughness	0.00007874	0.0020	0.00007874	0.0020	0.00007874	0.0020	7.87E-05	0.0020	0.00007874	0.0020
Center Freq. (GHz)	77.29		77.39		77.33		77.17		77.21	
Dk from Freq. Shift	Reference		0.008		0.003		-0.009		-0.006	

▲ **Table 1** Comparisons of the thru-coupled ring resonator and the thru-line edge coupled ring resonator in relation to variables which can potentially impact RF/microwave performance.

with a conductor and open circuit-board area, a narrower conductor results in more open circuit-board space. The far right-hand column of Table 1 shows the effects of a narrower ring conductor and resulting increased gap coupling space.

The Dk extraction is shown on the bottom row of Table 1 for each of the different scenarios. In summary, the thru gap coupled ring resonator has a worst-case Dk shift of 0.035. When subjected to the same material and process variations, the thru-line edge coupled ring resonator has a worst-case Dk shift of 0.009. This indicates that the thru-gap coupled ring resonator is more affected by material and PCB fabrication process variations in terms of RF performance than the thru-line edge coupled ring resonator.

Copper surface roughness is yet another circuit material quality that can affect the accuracy of material Dk characterization efforts. Copper surface roughness can impact transmission-line insertion loss and phase response at high frequencies.<sup>3</sup> The quality of the copper surface at the circuit material substrate-copper interface can affect the phase velocity of a high-frequency circuit's signals, with a rougher copper surface resulting in slower phase velocity. An EM wave with a slower phase velocity is an effect like a PCB material with an increase in Dk. Even if the Dk of a circuit substrate has not changed, if using circuits like ring resonators for Dk characterization, circuits with smoother copper will exhibit a circuit-perceived Dk or Design Dk that is lower than the same

circuits having a rougher copper surface.

In addition, a rougher copper surface will result in increased conductor loss compared to a smoother copper surface. The increase is dependent upon frequency, substrate thickness, and the amount of copper surface roughness. The effects of copper surface roughness will be more pronounced for circuits on thinner substrates than for circuits on thicker substrates. When evaluating the effects of copper surface roughness on insertion loss at lower frequencies with thick skin depth, the effects will be minimal compared to the more significant effects on loss at higher frequencies with thinner skin depth.

Circuit material copper surface roughness effects can impact the values of Dk and Df extracted from ring resonator circuits. Some amount of surface roughness is to be expected, although it is hoped to be within normal limits. Variations in roughness will occur within a single sheet of copper foil and from sheet to sheet, although for some copper, such as rolled copper, the surface roughness variations will be minimal. For standard ED copper, the normal surface roughness can have significant variation. For example, ED copper with a specified average surface roughness of 2.0  $\mu\text{m}$  RMS can vary as much as 1.8 to 2.2  $\mu\text{m}$  within the same sheet of copper.

Since a microstrip ring resonator has two substrate-copper interfaces, it is unlikely that the signal plane copper surface roughness will be the same as the ground plane for most copper types. If a RF/microwave engineer was trying to account for the effects of copper sur-

face roughness during material Dk and Df extraction, not having the same copper roughness on each interface is problematic and unpredictable. It is generally assumed that the signal plane copper surface roughness has more impact on RF performance than the ground plane copper surface roughness. The copper surface roughness can vary within a small area and the roughness for the ring conductor may vary and it may not be what is assumed.

The copper surface roughness must be part of any extraction process for Dk and Df using circuit structures such as ring resonators because of the impact of the copper surface roughness on test circuit performance. Errors due to copper surface roughness can be minimized by using rolled copper. It is smooth, with minimal variations in surface roughness, and minimal effect on phase or insertion loss of transmission lines in test circuits.

Ring oscillators can be effective test devices for extracting material Dk and Df at microwave frequencies; however, accurate extraction of Dk and Df at mmWave frequencies can be very challenging. Ring resonators are assumed to have no radiation since the ring is a closed structure, but there are always exceptions. For a tightly coupled ring resonator that is a thru-coupled resonator, the radiation in the gap coupled area can affect the quality factor (Q) of the resonator which can cause errors in Df extraction.

## SIW TEST CIRCUITS

As circuits move higher in frequency, substrate integrated waveguide (SIW) transmission lines are being used more in support of PCB-based mmWave applications. SIW provides some benefits at mmWave frequencies, although there are also some concerns when using this type of circuit structure for the extraction of material Dk and Df values.

Several methods can be used to extract Dk from a material with an SIW structure. One technique is based on using the 3-dB cutoff frequency of the SIW to extract the Dk of the circuit material. Another method involves phase angle measurements in the passband frequency range of the SIW to extract the Dk of the material. When using SIW structures at mmWave frequencies, the location of drilled holes in the circuit material must be extremely precise. Most PCB fabricators can hold a drilled hole location tolerance within  $\pm 1$  mil, which is considered good. But because the hole patterns form the sidewalls of the SIW, any variations in the hole spacings or locations can make a difference in the 3-dB cutoff frequency, especially at mmWave frequencies.

As an example, for an SIW designed for a 3-dB cutoff frequency of 70 GHz using a 5-mil-thick substrate with Dk of 3.0, a variation in wall hole location of 1 mil (one-half of the  $\pm 1$  mil tolerance) will change the 3-dB cutoff frequency by 1.5 GHz. If this frequency shift is assumed to be due to Dk only and not the SIW drilled hole tolerance, it will result in a shift/error of 0.12 in the extracted Dk value.

In addition, the 3-dB cutoff frequency of transitions of other transmission-line technologies to SIW can be sensitive to circuit fabrication variables. Transitions may be from microstrip to SIW or GCPW transmission lines to SIW. A microstrip-to-SIW transition is less affected by PCB fabrication variations than a GCPW-to-SIW transition. Multiple PCB fabrication variables can impact the RF performance of GCPW and these variations can certainly impact the 3-dB cutoff point. Because of these issues, extracting the Dk of the material by using the 3-dB cutoff frequency for SIW at mmWave frequencies is not recommended.

The phase angle response for the SIW in the passband frequency region is somewhat less sensitive to the drill location tolerance but it is still a concern. One design trick which could be advantageous for phase measurements in the passband for SIW is to use a dual row of grounding vias for each sidewall of the SIW structure. The drilled hole location tolerance requirement will still exist but having dual rows for each sidewall seems to give an averaging effect and minimizes the impact of variations in hole location on phase response.

Specific recommendations for measurements that can help determine circuit material Dk and Df at mmWave frequencies have not been made in either part 1 or part 2 of this article mainly because an industry-defined standard test method does not exist at mmWave frequencies (30 to 300 GHz). Different methods are available, although caveats must be made regarding accuracy under certain conditions. Measurements based on ring resonators have great value at mmWave frequencies but, without understanding the many variables related to these circuit structures, the accuracy of test results and Dk and Df characterizations can be greatly compromised.

---

## References

1. John Coonrod, "Managing Circuit Materials at mmWave Frequencies," *Microwave Journal*, Vol. 58, No. 7, July 2015.
2. Sonnet® Software Inc., <http://www.sonnetsoftware.com/>
3. Allen F. Horn, III<sup>1</sup>, John W. Reynolds<sup>1</sup>, and James C Rautio<sup>2</sup>, "Conductor Profile Effects on the Propagation Constant of Microstrip Transmission Lines," 1-Rogers Corporation, 2-Sonnet Software, IEEE Transactions on Microwave Theory & Techniques Symposium, 2010.

# 5G: Higher Frequencies!

## Do you have the **right** circuit materials?

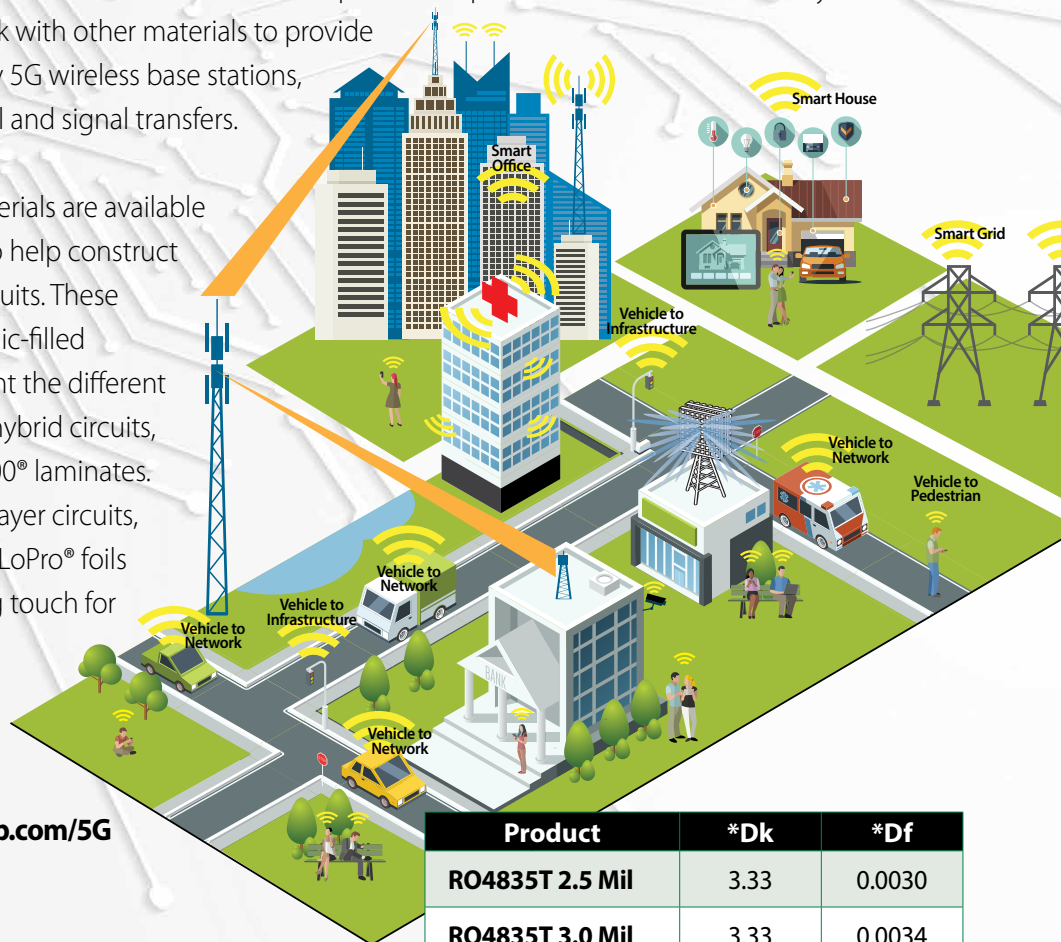
Frequencies at 28 GHz and higher are being used in Fifth Generation (5G) wireless communications networks. 5G infrastructure depends on low-loss circuit materials engineered for high frequencies, materials such as RO4835T™ laminates and RO4450T™ bonding materials from Rogers Corporation!

Rogers RO4835T spread-glass-reinforced, ceramic-filled laminates are low-loss materials in 2.5, 3.0, and 4.0 mil thicknesses. They are well suited for millimeter-wave frequencies as part of the inner cores of 5G hybrid multilayer PCBs. They can work with other materials to provide the many functions needed by 5G wireless base stations, including power, signal control and signal transfers.

Rogers RO4450T bonding materials are available in 3, 4, and 5 mil thicknesses to help construct those 5G hybrid multilayer circuits. These spread-glass-reinforced, ceramic-filled bonding materials complement the different materials that will form these hybrid circuits, including RO4835T and RO4000® laminates. And for many 5G hybrid multilayer circuits, Rogers CU4000™ and CU4000 LoPro® foils will provide a suitable finishing touch for many hybrid multilayer circuit foil lamination designs.

**5G is here! Do you have the right circuit materials?**

Learn more at [www.rogerscorp.com/5G](http://www.rogerscorp.com/5G)



Product	*Dk	*Df
RO4835T 2.5 Mil	3.33	0.0030
RO4835T 3.0 Mil	3.33	0.0034
RO4835T 4.0 Mil	3.32	0.0036
RO4450T 3.0 Mil	3.23	0.0039
RO4450T 4.0 Mil	3.35	0.0040
RO4450T 5.0 Mil	3.28	0.0038

\* IPC TM-650 2.5.5.5 Clamped Stripline at 10 GHz - 23°C



Advanced Connectivity Solutions

USA - AZ, tel. +1 480-961-1382 • EUROPE - BELGIUM, tel. +32 9 235 3611  
[www.rogerscorp.com](http://www.rogerscorp.com)

